2. Blasting work experiences

Stockholm Conference Proceedings 2017, R. Holmberg et al

Controlled explosive demolition of a mineral processing plant at Mantoudi (Greece) - Stage 2 of the project: rotary kilns and concrete structures

E. Baliktsis, A. Baliktsis & S. Baliktsis
Engineers of EXORIXI SA, Serres, Greece

ABSTRACT: On 2 July 2015 EXORIXI SA completed a progressive 'controlled explosive demolition' (CED) of the six rotary kilns and concrete structures at an old industrial minerals (magnesite) processing plant at Mantoudi, Greece. This, the second stage of a wider project, followed the controlled explosive demolition of six buildings, carried out by the same company in December 2013. A total of six rotary, horizontal kilns were installed and operated until 1998, constituting the heart of a well-known mineral (magnesia) production plant. A variety of concrete structures were included in the CED programme after the removal of metal parts and machinery: four tall buildings on the feeding side, four tall buildings on the output side of the kilns and 30 concrete blocks (plinths), supporting the kilns and their mechanism. Existing operating industrial facilities and preservable historic structures in the vicinity of the plant had to be protected. All works took into account the limited availability of flyrock cover protection means, supporting and preparation works, machinery and budget. For these reasons, the execution of the work lasted three months, and demolitions progressed step by step. Approximately 35 blasts were required for the demolition of all concrete structures, leaving the four high buildings on the feeding side to be the last demolished. Working parameters and details had to be adapted according to the characteristics of the specific structure of the demolition procedure. All demolition works progressed flawlessly, with no damage to the surrounding area and preservable buildings, and very low, completely acceptable vibrations. Evidence, risk and restriction parameters as well as practical knowledge and adaptations and differentiation from this controlled explosive demolition project, are presented in this paper.

1 THE MANTOUDI CONTROLLED EXPLOSIVE DEMOLITION PROJECT

Stage 1 of this project was the CED of six buildings and was carried out inside the mineral (magnesite) processing plant at Mantoudi, Evia, Central Greece (Figure 1), on 19 December 2013.

The buildings demolished were regarded as heavy industrial structures of reinforced concrete, concrete silos and concrete bases for heavy steel silos, with heights, ranging from 7 up to 40 m. Additionally, a 45 m high, steel chimney was also demolished. The minimum distance of 1.8 m between the highest building to be demolished and the closest building that had to remain intact highlights how challenging this project was. The 36 m high building, had to be protected from any damage, as it contained the old HERRESHOF, that is 7.5 m in diameter and 16 decks vertical, shaft furnace of the caustic calcined magnesite (CCM) production line (Figure 2). This was scheduled to be repaired and gradually incorporated in the production complex of the new investment. Indeed, the 'bet' was won and the

operation was successful: not only did it survive the demolition of surrounding structures, but its maintenance was completed quickly, and it is currently part of the operating production process. It includes 16 decks, for a maximum operating temperature of 1000ºC, annual production capacity of 60,000 tons CCM, or feeding capacity of 132,000 tons magnesite (as raw material).

Figure 1. View of the area of the controlled explosive demolition project in Mantoudi, Evia, Central Greece.

On 2 July 2015 EXORIXI SA completed a lengthy progressive CED of the six rotary kilns, facilities and concrete structures of the old industrial minerals (magnesite) processing plant at Mantoudi, Greece, near the site of Stage 1. Stage 2 of the Project will be main theme of this paper.

2 DATA AND BASIC FACTS OF THE STRUCTURES AND THE SITE

The old plant was part of a big industrial complex, covering almost 300,000 m^2, constructed around 1970, and operated up to 200 by the company SKALISTIRIS - FIMISCO. TERNA MAG SA has been the owner of this plant, and also the new investor and operator, since 2009. The company was also engaged in primary – mining activities, with privately owned surface and underground magnesite mines. Its processed magnesia products were known and requested for their superior quality, and exports were the basic commercial activity.

This processing (calcining) plant was the heart of the magnesia production process. It included 6 rotary kilns (Figure 2), one shaft (vertical) kiln and some more small furnaces, some of which were constructed and started operating in the 1930s. During the installation and commencement of operation, it probably constituted one of the largest collections of industrial kilns of that type.

Figure 2. Drone camera view of the wider area of the magnesite processing plant. The focus is on the site and the structures related to Stage 2 of the project. The white building in the background is the HERRESHOF vertical kiln, after the controlled explosive demolition works of Stage 1.

The whole area is still named 'Fournoi', which is the Greek word for 'furnaces' or kilns.

A total of six rotary, horizontal kilns, from various manufacturers (including FLC, SMIDTH, NIKEX, etc.), were installed and operated from 1970 - 1972 until 1998 - 2000 (Figure 3). They constituted the heart of a globally well-known mineral (magnesia) production plant. For the purposes of this paper, the kilns were designated as T1 - T6 according to their construction and operation series, as depicted on Figure 4. The feeding part and the chimney of T1 had to remain intact as a 'museum' item, even though it was in very bad condition due to its age. Furthermore, the feeding part of T2 had been partially removed some years ago by contractors in an attempt to recover metal parts.

A variety of concrete structures were included in the CED program of Stage 2 (Figures 4, 5, 6). The removal of the main metal parts and machinery paved the way: four 40 m tall buildings on the feeding side (coded as T31, T41/T46, T51/T56 and T61), four 20 m tall buildings on the output side of the kilns (T37, T47, T57 and T65) and almost 30 massive concrete blocks (plinths) between them, of up to 11 m height and 300 m^3 each, supporting the kilns and their rotating mechanisms. These blocks were very heavy with strong concrete elements, with rebars and large diameter anchors. What is more, some very heavy rotation parts (rings) (such as the head and end devices of the kilns as can be seen on Figures 13, 14, 15) remained on-site in order to be dropped down to the ground after blasting and concrete supports removal.

Existing operating industrial facilities and preservable, historic structures (some of which were under the supervision of the Archaeological Service, like T1) in the vicinity of the plant had to be protected.

All works had to be implemented on the basis of limited availability of flyrock cover protection means (as referred in the following), supporting works, lack of machinery in the area and low budget (it's remarkable that the country had entered into an intense economic crisis with implications for banking and projects budgets and cash-flows). EXORIXI SA had to adapt to these

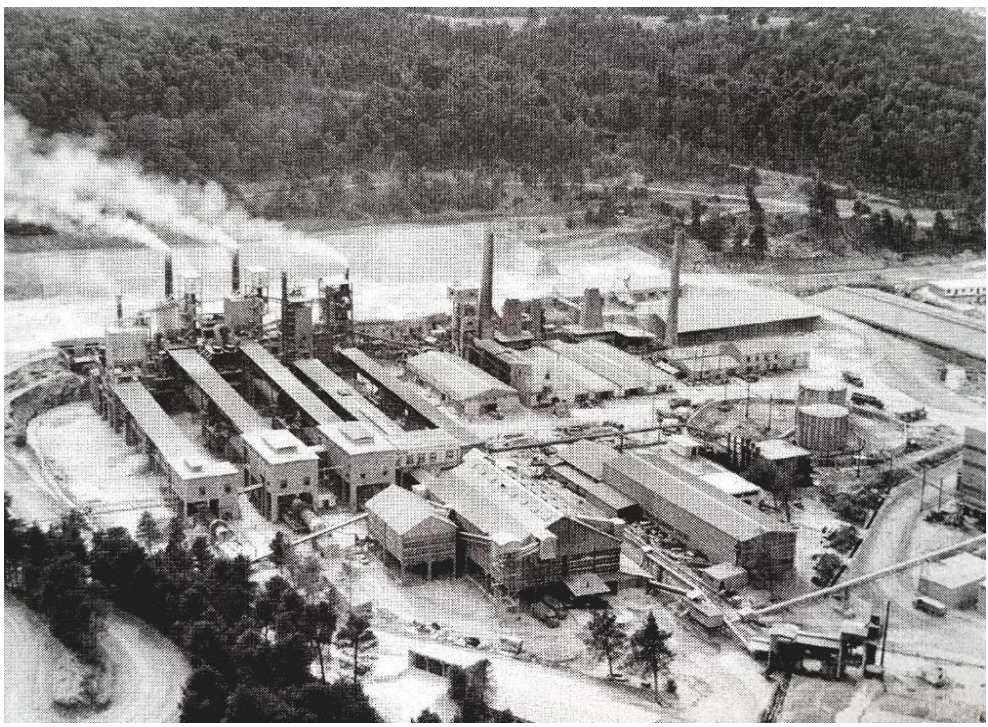

Figure 3. Historic photo with a panoramic view of the 6 rotary kilns and supporting facilities. It was published around 1972-75, when the SKALISTIRIS - FIMISCO group was enjoying its peak performance and fame, and the industrial plant was working at full productive capacity.

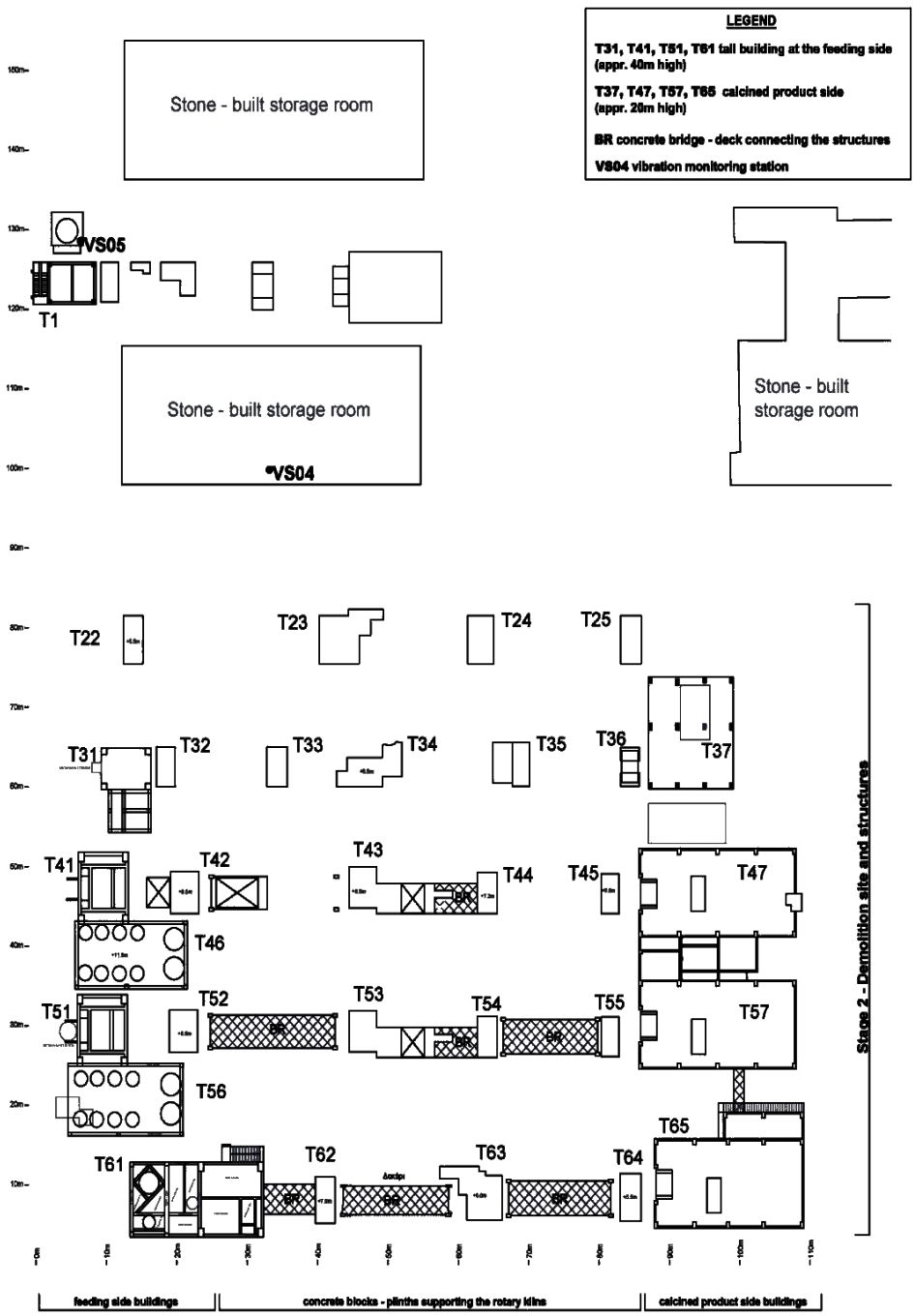

Figure 4. Plan view of the structures in Stage 2.
The vibration monitoring stations (VS04, VS05) are also depicted.

Figure 5. Drone camera view of the buildings to be demolished during Stage 2. The photo was taken during the first day of the demolition project. The T6 rotary kiln was yet to be completely removed.

Figure 6. Partial view of the site. On the right the tall buildings on the feeding side. The T6 rotary kiln was yet to be completely removed. The metal structure on the top of concrete blocks (some of them weighting more than 5 tons), were anchored in the concrete and used as a base for the rotary kilns sitting on them along with the rotation and braking mechanism.

conditions, retaining the flexibility to overcome such problems and implement the explosive demolition planning.

The tall buildings (mainly T31) were in bad condition, and in some cases it was difficult to approach them, not to mention entering and working inside them. As a ground rule, these structures had to be protected from every single blast close to them (which was the case for adjacent structures, such as T32, T36, T42, T52).

For these reasons, the works lasted almost three months, and demolitions progressed step by step. A kind of priority list had been established and demolition blasting works were implemented in the following order:

- supporting concrete blocks, initial works in order to create drop zones for the tall buildings and open the area aiming to provide better working conditions for the machinery dealing with the demolition, debris removal, cranes approaching, etc. (T22 – T25 structures were blasted last, in order to partially contribute to flyrock protection)
- end side buildings (T37, T47, T57, T65)
- final blasting (end of day on 2 July 2015) of the tall structures on the feeding side (T31, T41/T46, T51/T56 and T61)

3 DRILLING AND BLASTING

Hand-held drills were used to prepare almost 2200 blastholes. Drilling diameter was either 40/45 mm or 32/34 mm (for the cases of using 'non-explosive' materials, as referred in the following). Drilling depth varied from 0.40 to 5.00 m. Vertical and inclined long blastholes were used in the concrete plinths.

We designed and utilised a special drilling system in order to prepare and accelerate the preparation of (horizontal and with a slight upwards inclination) blastholes at the lower part of the concrete support plinths. This system proved to be a practical and efficient solution. This is due to the absence of alternative solutions of drilling machines, while it facilitated the work of drillers, providing simultaneously better time and risk management. It was based on our previous experience of drilling systems used in marble stone quarrying (Figures 7, 8).

Blasting gelatin and (limited quantities of) emulsions, in cartridges of 28 or 32 mm diameter, were used for charging the blastholes. The total quantity was around 2,000 kg.

The majority of blastholes and explosives (charges) were in the concrete plinths. It is significant that the demolition of the 4 tall buildings of the feeding side (T31, T41/T46, T51/T56 and T61) was based on less than 200 kg of gelatin.

The initiation system as well as the definition of delay times was based on non-electric detonators.

Figure 7. Drilling at the lower part of concrete block T45.

The allocation of delay times of the 4 tall buildings on the feeding side during the planning of the initiation system, was performed by taking into consideration a simultaneous demolition of all buildings, but in a 'synchronized' way. That refers to a pre-defined initiation and time sequence, as well as on a predesigned falling zone and drop direction for each one. As all buildings were close to each other, what had to be assured was that no one of them would cause any problem for the falling movement of its adjacent structures.

What is more, in order to avoid some tall buildings turning into dangerous sites that one cannot approach or enter (due to explosive demolition of some nearby structures), the decision was taken to use pyrotechnic material ('non-explosives'). In this manner, this solution

Figure 8. Drilling at the lower part of concrete block T45.

was applied in the case of structures T32, T37, connecting concrete bridges and decks between T61 - T65, as well as some concrete plinths inside the buildings T47 and T57.

4 FLYROCK RISK

It was rather difficult if not impossible to apply flyrock cover protection everywhere. The blasting of T2 structures was delayed as it was considered that these could probably form an indirect 'protection wall' for the nearby old stone built buildings.

Instead of using flyrock cover protection, there was a systematic approach and consideration of the following:

- Meticulous management of each blasthole's direction during design, planning and drilling. In this way, the remaining flyrock risk was in a way directed towards the area of less interest regarding possible damaging effects.
- On the same principle, only light charges, and only a small number of blastholes were used in the upper parts of the buildings, especially where the concrete elements and dimensions allowed so, or their condition was poor.
- Stemming with foam was implemented in all blastholes.
- Cover protection was used on the T31 building. Wire fencing and strong geotextile were placed on the sides towards T1 and the nearby stone-built storage facilities (Figure 15).
- Specially prepared heavy metal sheets were systematically used, mainly for the blasting of concrete plinths (Figures 9-12). These heavy sheets were available on-site from the metal parts and machinery removal during the preparation of the facilities. These were moved on a repeated basis by a big wheel loader and for each blasting session were placed on the side with highest risk. Even though it was initially considered as a rather drastic measure, it finally proved to be a very effective solution. The project's flyrock management was deemed entirely successful, as there were no relevant damages.

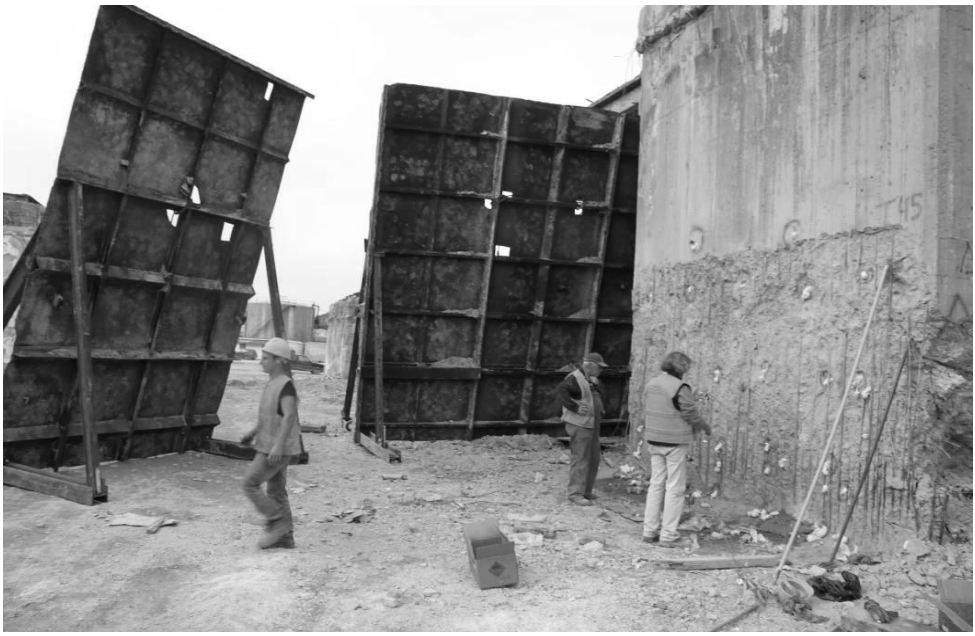

Figure 9. Charging at the lower part of concrete block T45. The metal sheets served to minimize flyrock.

Figure 10. After the blasting of concrete block T45. The metal sheets helped to minimize flyrock.

Figure 11. Completion of preparation works at concrete block T24. The metal sheets served as a way to minimize flyrock.

Figure 12. After the blasting of concrete block T24 (as on Figure 11). The metal sheets helped to minimize flyrock avoiding damage to the nearby stone-built storage room.

5 THE BLOW-DOWN PROGRAM

Approximately 35 ‘blasting days’ were required for the demolition of all concrete structures, leaving the four high buildings on the feeding side (T31, T41/T46, T51/T56 and T61) to be demolished last. This step-by-step operation, therefore, regarded a flexible and reproduced program of works.

An action plan and sequence of works for each demolition day was formulated and presented to the working groups and authorities involved, as well as the staff of the company - employer. Detailed sequence of events, allocation of responsibilities and safety positions for everyone involved in the demolition procedure were included in the Action and Safety Plan, ensuring the smooth and precise completion of works. All teams that had a role in this operation were coordinated according to this action plan.

Figure 13. Completion of preparation work at tall building T51 on the feeding side. Heavy metal parts like the feeding head of the kiln, remained in the building.

A team also staffed the Control Point for the last day demolition of the four high buildings on the feeding side. That team had the general responsibility for the implementation - progress and proper execution of the action plan, as well as the implementation and controlling of the exclusion - safety zones.

For each demolition day, the firing time was chosen to enable the temporary evacuation of the area around the demolition site of workers and contractors’ teams. The last demolition day was a non-working day for the production facility.

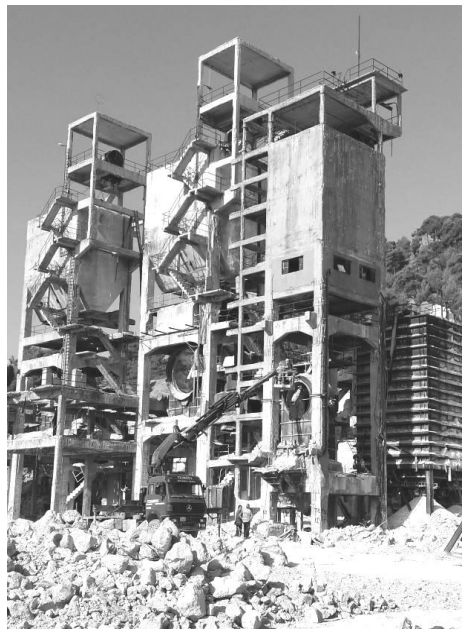

Figure 14. Completion of preparation work at tall building T31 on the feeding side. The next two tall buildings are T41 and T51. A crane was necessary, as entering the buildings was very risky.

6 VIBRATIONS MONITORING PROGRAMME

A monitoring programme was implemented for the demolition induced blast vibrations, with a network of two digital vibration monitors (seismographs). The processing of the data coming from this network referred to the vibrations ‘felt’ by the old T1 structure (monitoring station coded as VS05) and the closest stone built storage building near the T2 plinths (VS04), as depicted on Figure 3.

The vibration velocity (PPV) values were so low, that they would actually be acceptable for the benchmark in an inhabited area. Maximum ground vibration velocity values (PPV) were 1.65 for the VS05 and 9.63 mm/sec for the VS04 caused by the blasting of the closest T23. The values were commented as acceptable according to the

Figure 15. The T31, T41, T51, T61 tall buildings on the feeding side a few minutes before blasting. Flyrock cover protection was used only on limited charging places around T31 and can be seen on the right.

Figure 16. The T31, T41, T51, T61 tall buildings on the feeding side a few minutes after blasting.

DIN4150 specifications for L2 / L3 type of structures.

7 VIDEO RECORDING

This step-by-step operation involved a variety of concrete structures and imposed a continuous differentiation and manipulation of the explosive demolition procedure. Hence our intention to keep records for post evaluation and review of the whole process.

On each demolition day, photo and video cameras, one high speed video camera and also a drone (UAV) with a camera on board were in operation. In addition, a camera operating in time-lapse mode had been installed on the tallest point of the site, which was the T61 front (drop) side.

The availability of these recordings and respective analysis of the data made a considerable contribution to the project. Besides the impressive character of this visual material, it offered practical benefits and was utilized during the day to day operations in order to improve the blast design of the concrete plinths, to check and document the accuracy of the detonators and delay elements, to follow and evaluate the flyrock events, etc.

8 CONCLUSIONS

Stage 1 of the Mantoudi industrial facilities CED project concerned 6 buildings in one blasting operation. Stage 2 concerned 30 massive concrete blocks (plinths), 4 buildings of 20 m height and 4 buildings of 40 m height. A total of 35 'blasting days' and blow-down operations were required in order to complete this job. The CED of 4 tall buildings on the feeding side on 2 July 2015 was the concluding operation of the blown-down procedure (Figures 15 and 16).

Technical parameters of the site and national economic conditions imposed the step-by-step demolition of the concrete facilities and the gradual implementation of the blown-down program. This was the basic difference in comparison to the Stage 1 CED of December 2013. What is more, it was a practical demonstration and confirmation that CED technique provides flexibility and opportunities for adaptation on local conditions and availability of machinery and budget.

The three months CED working programme was utterly successful, safe and progressed in the designed way, exactly as scheduled. Although its lengthy duration was imposed by the existing technical and economic conditions, it provided the opportunity to improve the preparation and implementation parameters of blasting technique, mainly with regard to the concrete blocks, which consumed almost 80% of drilling works and explosives.

The whole management and control of responsibilities of the project included the study and design of the demolition works, the charging as well as the implementation of complex and extended firing systems. In addition, the management of all actions on the blasting days, the vibration monitoring, video documentation (using a great number of video cameras, among others a high-speed video camera and a camera mounted on a drone/UAV). At the same time, a significant part of the contracting works concerned the preparation of the buildings for the demolition as well as all drilling and charging works inside the structures, where working conditions were risky, nearly prohibitive, even for the very access of the workers.

Some important and useful experience that can constitute a powerful tool for similar projects refers to the fact that with a detailed planning - design, effective risk management and proper implementation of working parameters, we can conclude that:

- many different preparation works can be applied on the same site and on nearby structures, even if that means drilling can coincide with blasting (of nearby ones)
- limited availability of machinery and means could impose alternatives for effective handling of the needs and adaptation to the working conditions (e.g. drilling at the lower part of concrete plinths and using flyrock protection by heavy metal sheets)
- a number of structures can be demolished efficiently and safely in a synchronized way; lessons learnt from the Stage 1 CED of December 2013 were successfully reapplied on the 4 tall buildings of the feeding side on the last blasting day of Stage 2 (2 July 2015).

REFERENCES

Baliktsis, E., Baliktsis, A., Baliktsis, S., & Moran, C. 2015. Synchronized controlled explosive demolition of six industrial buildings at Mandoudi, Greece. *8th EFEE World Conference on Explosives and Blasting; Proc. Inter. Conf, Lyon, France, 26-28 April 2015.*

EXORIXI SA, 2015. Work Method Statement. *Un-published, submitted and presented to the Employer*.

EXORIXI SA, 2015. Summary Report on the vibration monitoring program of each demolition day. *Un-published, submitted to the Employer*.

EXORIXI's *web-page* (www.exorixi.gr).

TERNA MAG *web-page* (www.ternamag.com).

EXORIXI SA, 2013 – 2016. Video – presentation on YouTube (key words: EXORIXI MANTOUDI).

Pantazis, S. 2015. History of the SKALISTIRIS family and the relative corporate business activities (FIMISCO Company).

Stockholm Conference Proceedings 2017, R. Holmberg et al

Dynamic response of a defective slope under open-pit to underground mining blasting

C.B. Zhou, S.W. Lu & N. Jiang
Faculty of Engineering, China University of Geosciences, Wuhan, China

ABSTRACT: The characteristic of sublevel caving induced blast loadings is firstly analysed through LSDYNA. Then a three-dimensional numerical model with a potential sliding plane is established and the distribution of peak particle velocity (PPV) is analysed by inputting the obtained blast loadings. Finally, based on the stress wave theory, the formula of critical PPV is derived. Results show that: (1) on the slope surface, horizontal and vertical PPVs decrease but the attenuation rate changes greatly near the sliding plane; (2) on the whole, PPV in the rock mass above the potential sliding plane is greater than that below the plane; (3) the slope face can obviously amplify the horizontal PPV compared with the vertical PPV; (4) the safety criterion is analysed and the safety threshold is proposed. KEYWORD: open-pit to underground mining; defective slope; blasting vibration; safety criterion.

1 INTRODUCTION

With the continuous exploitation of near-surface mineral resources in China, the open-pit mining slopes continue to become higher and steeper, whose stability is declining. Because of the depletion of near-surface mineral resources and increasing mining, underground mining will be adopted in more and more mines in the condition of high and steep slopes. As the necessary means in mining, rock excavation and other constructions, blasting brings huge benefits, on the other hand, blasting-induced landslides, collapses and other geological disasters are nothing new across the world.

In recent years, extensive researches on slopes subjected to open-pit to underground mining have been conducted all over the world and a lot of achievements have been obtained. Ausilioe *et al.* studied the seismic stability of reinforced slopes (Ausilioe *et al.*2000). Li *et al.* studied the seismic stability of rock slopes based on the limit analysis method (Li *et al.* 2009). Basha and Basudhar studied the seismic stability of reinforced soil structures (Basha & Basudhar 2010). Latha and Garaga analysed the stability of a rock slope in Himalayas (Latha & Garaga 2010). Deb *et al.* analysed the stability of a pit slope in Pasir coal mine under blast loading (Deb *et al.* 2011). Chen *et al.* analysed the dynamic stability of the high rock slopes at Jinping I Hydropower Station by the pseudo-static approach and the modified Sarma method (Chen *et al.* 2014). Kumar *et al.* studied the propagation of blast waves in rock mass and its

influence on rock stability (Kumar *et al.* 2015). But the focus of these researches is on the stress field and the displacement field. The propagation of blasting vibrations in open-pit to underground mining slopes and the safety criterion is rarely studied.

In this paper, the characteristic of sublevel caving induced blast loadings is firstly analysed through LSDYNA. Then a three-dimensional numerical model is established and the distribution of peak particle velocity (PPV) is analysed by inputting the obtained blast loadings. At last, based on the stress wave theory, the formula of critical PPV is derived.

2 BLAST LOADINGS OF SUBLEVEL CAVING

In order to study the characteristics of medium-long hole blast loadings in underground mining, a numerical model is established based on the actual situation of underground mining in Daye Iron Mine, as shown in Figures 1a and 1b. The dimensions of the model are 30m in height, 16m in width and 5m in thickness. The side surfaces except the backside are applied for non-reflection boundary. The backside surface and internal boundaries are free.

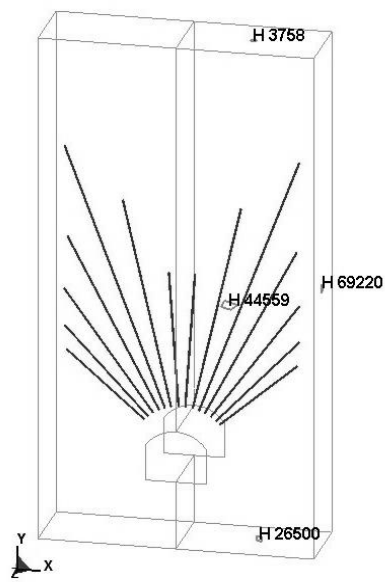

Figure 1a. Numerical model of sublevel caving - layout of blastholes.

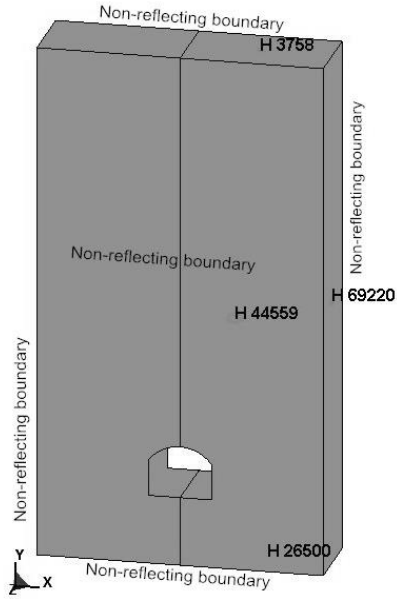

Figure 1b. Numerical model of sublevel caving - boundary conditions.

The Jones-Wilkens-Lee state equation can simulate the relationship between pressure and specific volume in the explosion process. The equation is as follows:

$$p_{eso} = A\left(1-\frac{\omega}{R_1 V}\right)e^{-R_1 V} + B\left(1-\frac{\omega}{R_2 V}\right)e^{-R_2 V} + \frac{\omega E_{0s}}{V} \quad (1)$$

where A, B, R_1, R_2, and W are material constants, p_{eso} is pressure, V is relative volume and E_{0s} is initial specific internal energy. The physical and mechanical parameters of the dynamite are the same with that of the field test and are listed in Table 1.

MAT_MOHR_COULOMB is chosen to simulate the constitutive relationship of surrounding rock. The physical and mechanical parameters are listed in Table 2.

Four elements are selected to analyse the blasting loads. The pressure-time curves are plotted in Figure 2.

It can be seen from Figure 2 that the peak pressure of each element is in the range of 1.9 - 43.05 MPa. The blasting loads reach its peak value at about 2 ms and then decrease dramatically before 14 ms. After 14 ms, the pressure is close to zero and varies little. So the pressure-time curves

Table 1. Mechanical parameters of explosives.

Density (g/cm^3)	D (cm/μs)	A (GPa)	B (GPa)	R_1	R_2	ω	E_{0s} (GPa)
1.09	0.4	214.4	18.2	4.2	0.9	0.15	4.192

Table 2. Mechanical parameters of surrounding rocks.

Density (g/cm^3)	Elastic modulus (GPa)	Poisson's ratio	Cohesion (MPa)	Friction angle (^{o})
4.12	12.5	0.27	0.337	40

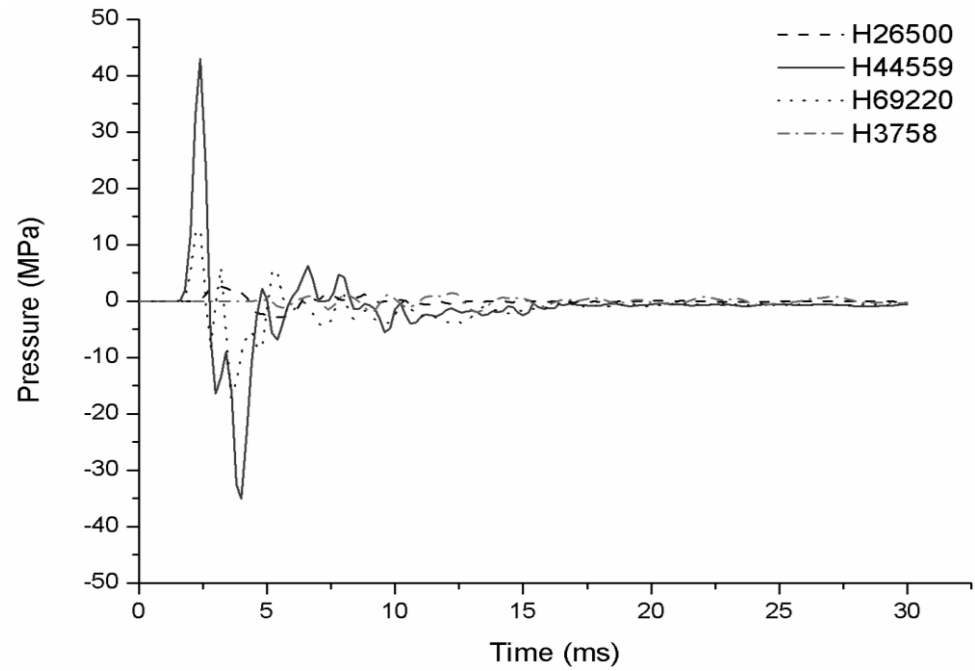

Figure 2. Pressure-time curves of selected elements.

before 14 ms can be regarded as the entire blast loading, which can be the input loading for further study.

3 PROPAGATION OF BLASTING VIBRATIONS

3.1 Numerical model

In order to analyse the influence of open pit to underground mining on the propagation of blasting vibrations, numerical models of different mining depths are established, as shown in Figures 3a and 3b. The model is 250 m in width by 250 m in height. The slope angle is 50^o and the slope height is 100 m. A potentially unstable block is formed by the sliding plane, whose dip angle is 30^o. Four cases of blasting positions at 36 m, 48 m, 60 m and 72 m above mean sea level (AMSL) are studied. The horizontal distance between the slope toe and blasting positions is 7 m.

The physical and mechanical parameters of the slope rock mass are the same with that in Section 2. The normal and shear stiffness of the sliding plane is 2 GPa/m, the cohesion is 0.128 MPa and the friction angle is 23°. The side surfaces and the bottom surface are applied for non-reflection boundary, and the top surfaces are free. For each mining depth, a cuboid cavity with the same dimensions in Section 2 is excavated and the obtained blast loadings are applied on the interior boundaries.

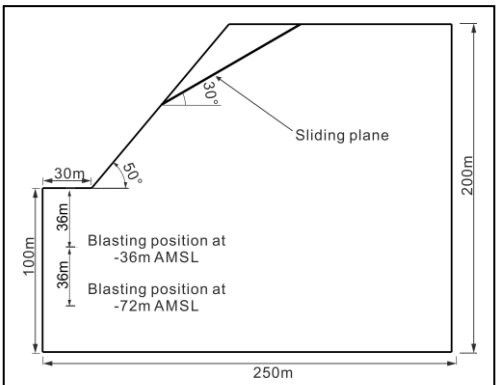

Figure 3a. Numerical model and its boundary conditions – dimensions.

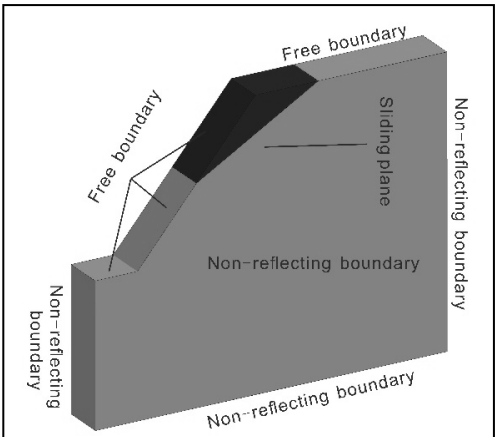

Figure 3b. Numerical model and its boundary conditions - boundary conditions.

3.2 Results and discussions

3.2.1 Propagation on slope surface

The monitoring points on the slope face is shown in Figure 4. Nine monitoring points are arranged on the slope face, numbered by S1, S2, S3, S4, S5, S6, S7, S8, S9. The vertical distance between adjacent monitoring points is 5 m.

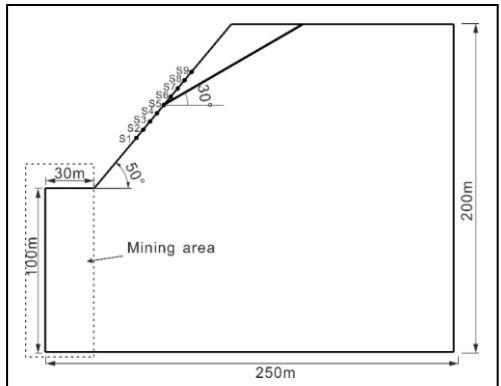

Figure 4. Monitoring points on the slope face

The distribution of horizontal and vertical PPVs for different mining depths are shown in Figures 5a and 5b.

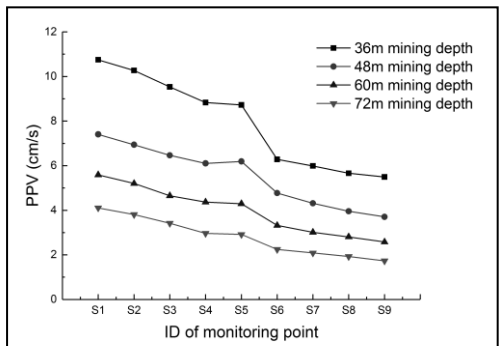

Figure 5a. PPVs distribution on the slope face - horizontal PPV.

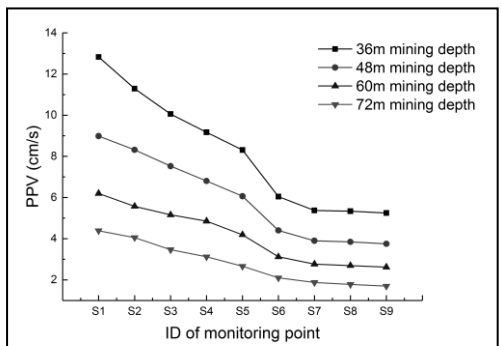

Figure 5b. PPVs distribution on the slope face - vertical PPV.

It can be seen from Figure 5 that PPVs decrease along the slope face and the horizontal PPV is less than the vertical PPV on the whole. The PPV attenuation rate decreases distinctly before the blasting seismic wave reaches the sliding plane and then increases rapidly. It may result from that the sliding plane may impede the propagation of the blasting seismic wave, and reflected and transmitted waves will be generated. The superposition of reflected and incident waves makes attenuation rate decrease distinctly and the transmitted waves makes the attenuation rate increase. Both horizontal and vertical PPVs decrease with the increasing mining depth. However, the distribution of PPVs is similar, which indicates that the mining depth has a quite small influence on it.

3.2.2 Propagation along sliding plane

The monitoring points along the sliding plane are shown in Figure 6. Ten monitoring points are arranged, in which five monitoring points are above the sliding plane numbered by A1, A2, A3, A4, A5, and five monitoring points are below the sliding plane numbered by B1, B2, B3, B4, B5. The vertical distance between adjacent monitoring points is 5 m on the same side. The vertical distance between two sets of monitoring points is 10 m.

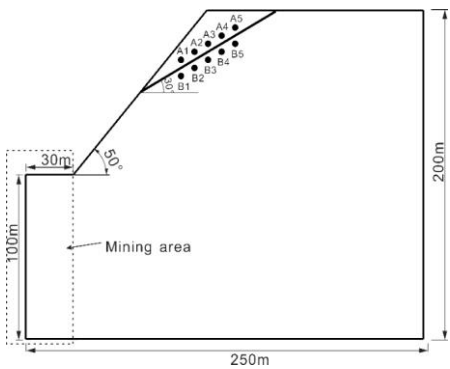

Figure 6. Monitoring points along the sliding plane.

The distribution of horizontal PPV above and below the sliding plane for different mining depths is shown in Figures 7a and 7b. The distribution of vertical PPV is shown in Figures 8a and 8b.

It can be seen from Figures 7 and Figures 8 that for different mining depths, the distribution of PPVs on both sides of the sliding plane is

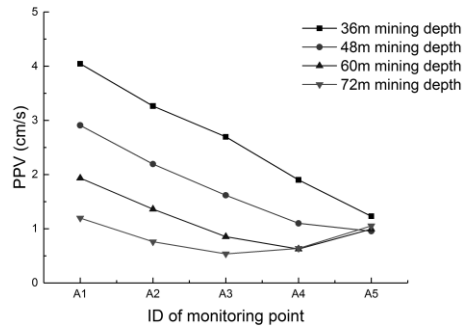

Figure 7a. Horizontal PPVs distribution along the sliding plane - above the structural plane.

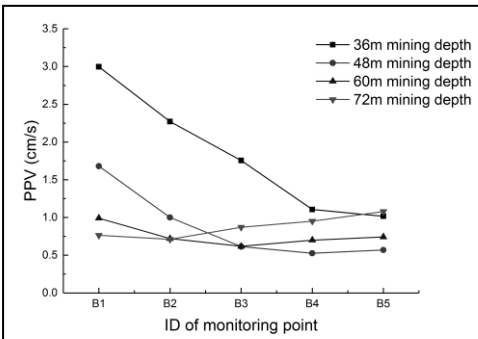

Figure 7b. Horizontal PPVs distribution along the sliding plane - below the structural plane.

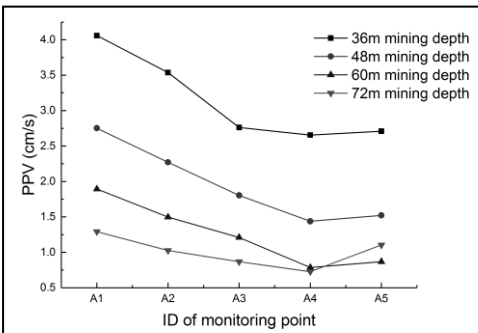

Figure 8a. Vertical PPVs distribution along the sliding plane - above the structural plane.

different. When the mining depth is 36 m and 48 m, PPVs on both sides decrease with the increasing ID (i.e. the increasing of both horizontal and vertical distance); when the mining depth is 60 m and 72 m, PPVs on both sides decrease first and then increase, but the positions of inflection points are not the same. Overall, the mining depth exerts a comparatively larger

influence on the distribution of PPVs and the PPV in the rock mass above the potential sliding plane is greater than that below the plane on the whole.

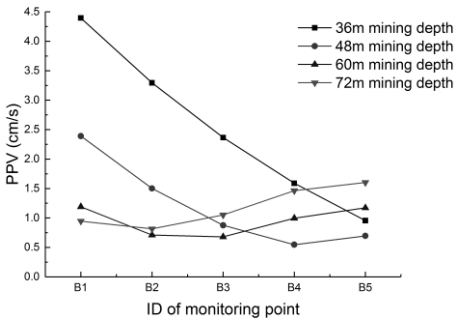

Figure 8b. Vertical PPVs distribution along the sliding plane - below the structural plane.

3.2.3 Propagation in vertical direction

The monitoring points in vertical direction are shown in Figure 9. Five monitoring points are arranged, which are numbered by D1, D2, D3, D4, D5. The vertical distance between adjacent monitoring points is 10m and the sliding plane is between D2 and D3.

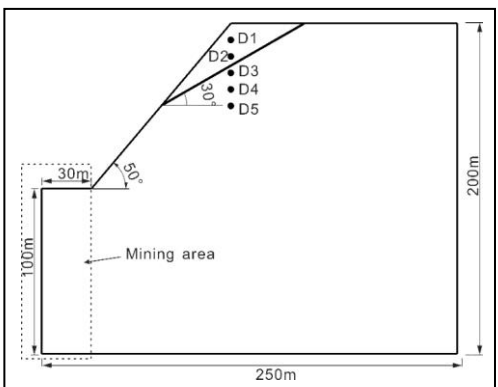

Figure 9. Monitoring points in vertical direction.

The distribution of horizontal and vertical PPVs for different mining depths are shown in Figures 10a and 10b.

It can be seen from Figures 10 that the distribution of horizontal and vertical PPVs changes distinctly with different mining depths, which indicates that the mining depth exerts a huge influence on the distribution of PPVs in the vertical direction. When the blasting seismic wave crosses the sliding plane from bottom to top, the horizontal and vertical PPVs increases if the mining depth is 36 m, 48 m and 60 m, but they decrease if the mining depth is 72 m. After the blasting seismic wave crosses the sliding plane, the horizontal PPV increases but the vertical PPV decreases. Compared with the vertical PPV, the slope face can obviously amplify the horizontal PPV in a certain range and its influence range decreases with the increasing mining depth.

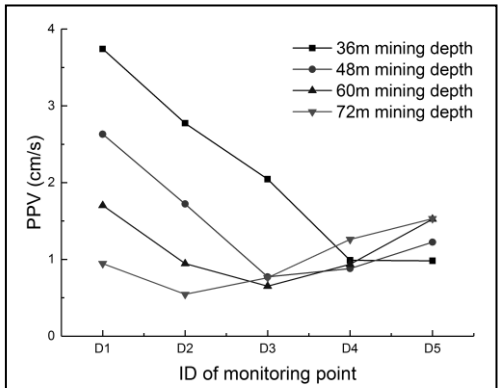

Figure 10a. PPVs distribution in the vertical direction - horizontal PPV.

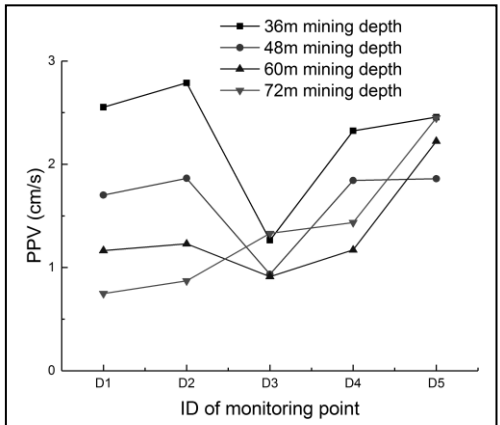

Figure 10b. PPVs distribution in the vertical direction - vertical PPV.

4 SAFETY CRITERION

When a plane stress wave is incident on the structural plane, new reflected and transmitted waves will generated. In order to study the reflections and transmissions, a coordinate system *Oxz* is set up, and $z=0$ is defined to be the

structural plane. The medium I is located in the region $z<0$, and the region $z>0$ represents the medium II.

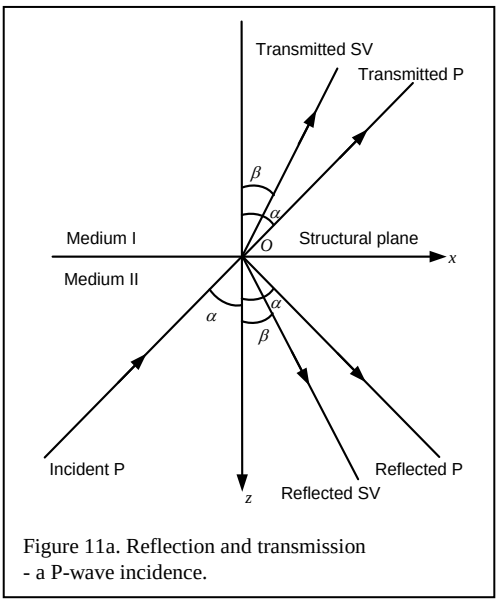

Figure 11a. Reflection and transmission - a P-wave incidence.

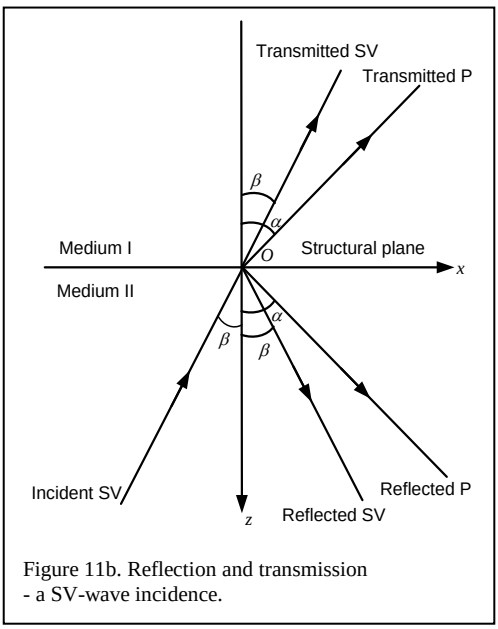

Figure 11b. Reflection and transmission - a SV-wave incidence.

Suppose a blasting stress wave is a plane harmonic wave, and the displacement potentials of a P-wave and a SV-wave can be written as:

$$\Phi_1 = A_1 \exp\left[i\omega\left(\frac{\sin\alpha}{C_p} x - \frac{\cos\alpha}{C_p} z - t \right)\right] \qquad (2)$$

$$\Psi_1 = B_1 \exp\left[i\omega\left(\frac{\sin\beta}{C_s} x - \frac{\cos\beta}{C_s} z - t \right)\right] \qquad (3)$$

where A_1 and B_1 are the amplitudes of the incident P- and SV-waves, ω is the angular frequency, C_p and C_s are the wave speeds of the incident P- and SV-waves, λ and μ are Lame constants, α and β are the incident angles of P- and SV-waves, t is time.

The reflection and transmission coefficients can only be obtained by considering the boundary conditions on the structural plane. According to the displacement discontinuity method, the stresses across and along the structural plane are continuous but the displacements are discontinuous. The constitutive relationship can be written as:

$$\begin{aligned} \sigma_{zz} &= k_n \Delta v \\ \sigma_{xz} &= k_t \Delta u \end{aligned} \qquad (4)$$

where k_n and k_t are normal and shear stiffness, Δv and Δu are the relative normal and shear displacements.

The model to calculate the safety criterion is shown in Figure 12, where H is the slope height, γ is the slope angle, h is the vertical distance between the bottom tip of the sliding plane and the top of the slope, W is the gravity of the potentially unstable block ABC, θ and l are the dip angle and the length of the sliding plane AC, C_h and φ are its cohesion and friction angle.

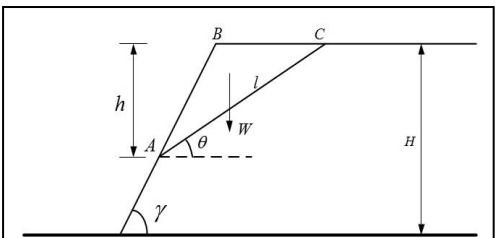

Figure 12. Calculation model for safety criterion

The gravity of block ABC $W = \frac{1}{2}\rho g h^2 (\cot\theta - \cot\gamma)$. Then the normal and shear forces can be written as:

$$\begin{aligned} F_n &= W\cos\theta - |\sigma_{zz}| l \\ F_\tau &= W\sin\theta + |\sigma_{xz}| l \end{aligned} \qquad (5)$$

The factor of stability K can be expressed as:

$$K = \frac{C_h l + F_n \tan\varphi}{F_\tau} \tag{6}$$

Finally, the critical PPV for an incident P-wave is given by:

$$\left|v_{1p}\right| = \frac{C_s\left(C_h l + W\cos\theta\tan\varphi - KW\sin\theta\right)}{l\left[\mu K\left|c\sin 2\alpha T_{P\to P} - \cos 2\beta T_{P\to S}\right| + \left|\lambda c\tan\varphi T_{P\to P} + \mu\sin 2\beta\tan\varphi T_{P\to S}\right|\right]} \tag{7}$$

The critical PPV for an incident SV-wave is given by:

$$\left|v_{1s}\right| = -\frac{C_s\left(C_h l + W\cos\theta\tan\varphi - KW\sin\theta\right)}{l\left[\mu K\left|c\sin 2\alpha T_{S\to P} - \cos 2\beta T_{S\to S}\right| + \left|\lambda c\tan\varphi T_{S\to P} + \mu\sin 2\beta\tan\varphi T_{S\to S}\right|\right]} \tag{8}$$

where $T_{P\to P}$ and $T_{P\to S}$ are the transmission coefficients for an incident P-wave, $T_{S\to P}$ and $T_{S\to S}$ are the transmission coefficients for an incident SV-wave, given by Gu *et al.*1996.

For the case of 36 m mining depth, the incident angle is 60° - 75°. We consider the critical state and K=1. Because the main frequency is about 100 Hz, we assume the main frequency of incident waves is 100 Hz. Then the critical PPV determined by Equations (7) and (8) is 3.12 cm/s. Although the slope is influenced greatly, it is still stable.

5 CONCLUSIONS

The following conclusions can be drawn:

- On the slope face, both the horizontal and vertical PPVs decreases, but the attenuation rate changes greatly near the sliding plane. It decreases distinctly before the blasting seismic wave reaches the sliding plane and then increases rapidly. Both horizontal and vertical PPVs decrease with the increasing mining depth, but the mining depth has a small influence on the distribution.
- Along the sliding plane, the mining depth exerts a comparatively larger influence on the distribution of PPVs, and the PPV in the rock mass above the potential sliding plane is greater than that below the plane on the whole.
- In the vertical direction, the mining depth exerts a huge influence on the distribution of horizontal and vertical PPVs. The slope face can obviously amplify the horizontal PPV compared with the vertical PPV, and its influence range decreases with the increasing mining depth.
- The formula of safety criterion is derived based on the stress wave theory and the displacement discontinuity method. The safety threshold of 3.12 cm/s in the case of 36 m mining depth is proposed. Although the slope is influenced greatly, it is still stable.

6 ACKNOWLEDGEMENTS

The study was sponsored by the National Natural Science Foundation of China (Grant No. 41372312), the Huanghe Yingcai (Science and Technology) program.

REFERENCES

Ausilio, E., Conte, E. & Dente, G. 2000. Seismic stability analysis of reinforced slopes. *Soil Dynamics and Earthquake Engineering*, 19(3): 159-172.

Basha, B.M. & Basudhar P.K. 2010. Pseudo static seismic stability analysis of reinforced soil structures. *Geotechnical and Geological Engineering* 28(6):745-762.

Chen, M., Lu, W., Yan, P. & Zhou, C. 2014. New method for dynamic stability analysis of rock slope under blasting vibration based on equivalent acceleration and Sarma method. *Canadian Geotechnical Journal* 51(4):214-215.

Deb, D., Kaushik, K.N.R., Choi, B.H., Ryu, C.H., Jung, Y.B. & Sunwoo, C. 2011. Stability assessment of a pit slope under blast loading: a case study of pasir coal mine. *Geotechnical and Geological Engineering* 29(4): 419-429.

Gu, B., Suárez-Rivera, R., Nihei, K.T. & Myer, L.R. 1996. Incidence of plane waves upon a fracture. *Journal of Geophysical Research* 101(B11):25337-25346.

Kumar, R., Choudhury, D. & Bhargava, K. 2015. Simulation of rock subjected to underground blast using FLAC3D. *Japanese Geotechnical Society Special Publication* 2(12): 508-511.

Li, A.J., Lyamin, A.V. & Merifield R.S. 2009. Seismic rock slope stability charts based on limit analysis methods. *Computers & Geotechnics* 36(1-2):135-148.

Latha, G.M. & Garaga, A. 2010. Stability analysis of a rock slope in Himalayas. *Geomechanics & Engineering* 2(2):125-140.

Stockholm Conference Proceedings 2017, R. Holmberg et al

Water blasting of steel box stanchions

I.R. Melzer
Project office of structural demolition, Dresden, Germany

ABSTRACT: Since 2001 a very elegant blast demolition method for hollow box steel stanchions in structures has been developed in Germany and is known as 'water blasting'. A correctly calculated charge of a detonating cord in a box stanchion filled with water cracks all edge welds easily. As a result the stanchion is completely destroyed. The charge weight depends not on the thickness of the box plates but only on the weld thickness. Such water blasting causes moderate influences to the surrounding. Importantly, by using this method no large pre-weakening of the stanchions is necessary. Forty-five large, power station steam boilers have already been blasted by this new method in Germany. Other power plant utilities like filter, buildings, silos and bunkers and complete steel plants could be tackled using this method too. The only requirement is hollow stanchions. The fundamental points of this method and some examples of spectacular blasts will be shown in this paper.

1 THE PRINCIPLE OF WATER FILLED STEEL BLASTING

In the past hollow iron columns were occasionally filled with water and small linear charges. The resulting blast was very effective. Around the year 2000, I thought 'why should we not do it with modern industrial steel stanchions?' If steel stanchions are hollow, like box columns or tubes, can't they be filled with water and blasted with a central-linear charge for example detonating cords?

The water carries the blast energy without loss. The central charge has to crack only the relatively small welding seams with the thickness 'a' and cracks the stanchion along the full length of the charge. The separated plates are no longer held together and they are bent out very easily. The stanchion is completely destroyed. The necessary charge weight is relatively small.

In the case of a tube stanchion the whole wall thickness has to crack. That is why tubes need more blast weight then box stanchions and the rest of the tube has more stiffness and stability than the plates.

Less appropriate for this technique are connected profiles such as H-Profiles or with additional plates see Figures 4 and 5. Their remaining stiffness after the blast remains fairly high.

Only one small circled hole on the top of the blast zone is necessary to fill water and explosive in. That is why a large pre-weakening is not necessary.

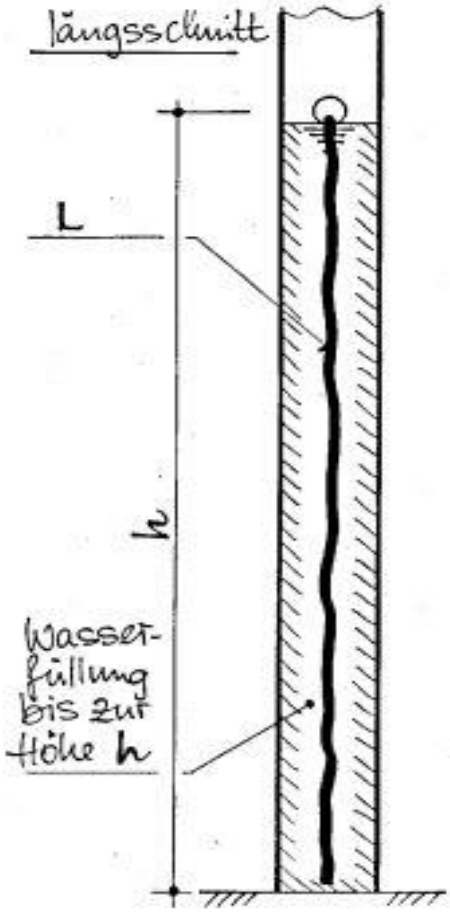

Figure 1. Water filled and charged steel box stanchion.

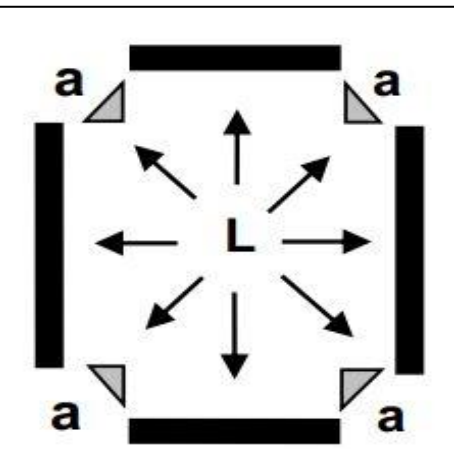

Figure 2. Water filled and blasted steel box stanchion.

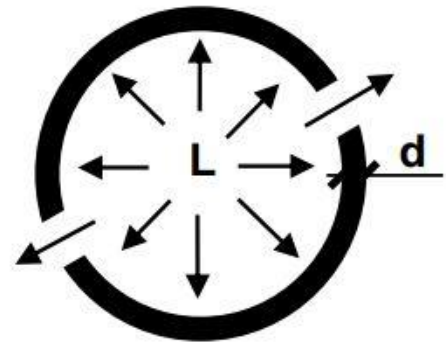

Figure 3. Water filled and blasted steel tube column.

Figure 4. Two or more H-profiles, suboptimal.

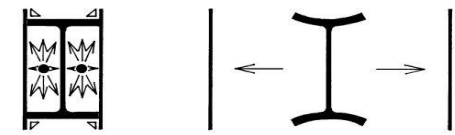

Figure 5. H-profile with plates, suboptimal.

2 TEST PHASE

In 1999 at a power plant in east Germany some tests of profiles, like H-H and U-U, took place to explore optimal load weights for water blasts. At this time we still thought that the load weight depends on the volume of the water filled in. These tests were continued in 2001 at another power plant (Hagenwerder). In the protection of an old shelter we applied several load weights in equal box stanchions (see Figures 6 and 7). But the optimal load weights are optimal for the used water volume only. We did not know any better at the time.

3 FIRST APPLICATIONS

In 2001 6 structures were water blasted and in 2003 a further 4 large steam boilers at power

Figure 6. Preparation of water blasting.

Figure 7. Good result of the test blast.

plants in Saxony were also water blasted. The 85 m tall boilers at Hagenwerder were each stood on 6 steel box stanchions with cross section areas of 1.8 m x 1.5 m. Four of these six stanchions were water filled and blasted to a height of 40 m. The only difficulty was making a trough (*sic*) hollow space in the stanchions. After the successful blast the separated plates of the stanchions were moving like noodles (see Figures 8 to 14).

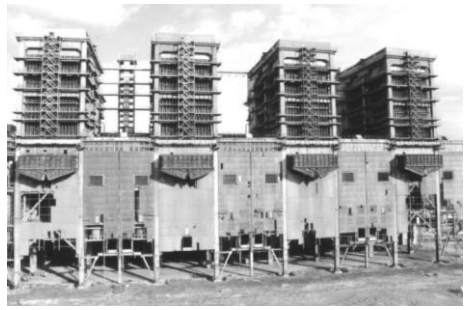

Figure 8. Boiler house, power plant Hagenwerder.

Figure 9. 40 m high reach stanchion water blast of the first boiler.

Figure 10. Boiler house from south.

The explosive used when water blasting the steel stanchions (Melzer 2004) had weights between 40 and 800 g/m. On occasions plate fly

was a problem. The furthest distance recorded was 126 m (see Figure 15). It is obvious the existing formula for determining the charge weight lacks reliability yet.

Figure 11. Boiler house tilting commences.

Figure 12. Boiler house is tilting underway.

Figure 13. Boiler house is tilting almost complete.

Figure 14. Foot of a box stanchion after the blast.

4 A BETTER LOAD WEIGHT FORMULA

All actual existing calculations of charge weights in blast demolition I know of were found empirically and not in clear physical relations. That is why in 2014 a research was started to get better formulas of load weights for blasting (Melzer 2015). The basic idea was that charge weights of steel water blasting does not depend on the water volume but only on the tensile resisting of the steel bandage, respectively its weakest member the edge welding - and of course of the performance of the explosive. For a water steel blasting I have derived the following simple formula:

$$L^* = ¶ \cdot Z^2 / S \qquad (1)$$

With
L* the load weight in kg/m,

Z the tensile strength of the bandage in MN/m; and
S the explosive power or 'blast strength' in $MN^2/(kg \cdot m)$.

$$S = p^2 / \rho L \quad (2)$$

p the explosion pressure [MN/m^2], and
ρL the explosive density [kg/m^3]

Example:
Eurodyn 2000: $S = p^2 / \rho L = 152.4^2 / 1400$
$S = 16.58\ MN^2/(kg \cdot m)$

The tensile force Z depends for welded boxes only on the welding seams with the thickness 'a' (see Figure 16) and the ultimate tensile stress σZ:

$$Z = \sigma Z \cdot a \quad (3)$$

Figure 15. Plate fly after water blasting.

Example:
Eurodyn 2000: $S = 16.58\ MN^2/(kg \cdot m)$, welds: a = 6 mm, $\sigma Z = 470\ MN/m^2$
$Z = 470 \cdot 0.006 = 2.82\ MN/m^2$; $L^* = ¶ \cdot \sigma Z^2 / S = ¶ \cdot 2.82^2 / 16.58 = 1.506$ kg/m

Example:
Eurodyn 2000: $S = 16.58\ MN^2/(kg \cdot m)$, tube: d = 10 mm, $\sigma Z = 470\ MN/m^2$
$Z = 470 \cdot 0{,}01 = 4.70\ MN/m^2$; $L^* = ¶ \cdot \sigma Z^2 / S = ¶ \cdot 4.70^2 / 16.58 = 4.185$ kg/m

This formula does not depends on the blast body volume. With it you can calculate the charges of water filled steel stanchions, water filled concrete stanchions or silos and other hollow structures.

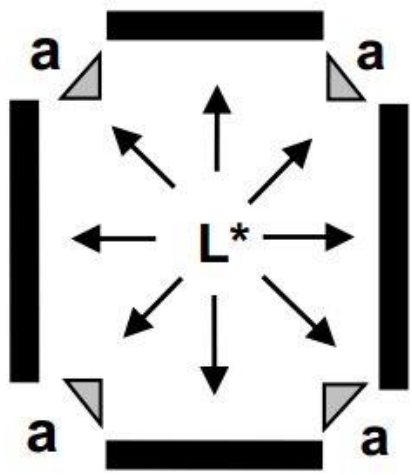

Figure 16. Water filled and blasted steel box stanchion.

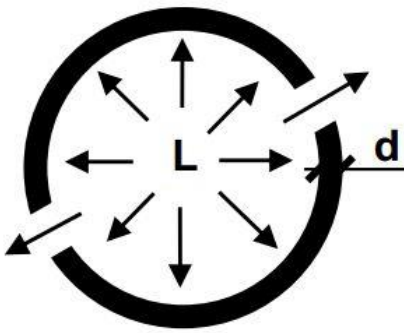

Figure 17. Water filled and blasted steel tube stanchion

5 LAST EXAMPLE

A large boiler house at the Thierbach power plant in Saxony was demolished by only using water blasting of the main stanchions supporting the boiler. The charge weight was determined using the new formula derived in 2015.

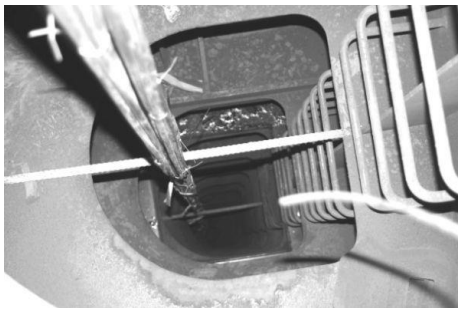

Figure 18. Charged inner of stanchion still without water.

Figure 19. Water blasting boiler stanchions Thierbach.

Figure 20. Boiler tilting.

In January 2015, the separate number 1 boiler was water-blasted. This was followed in February by the three remaining boilers (2 to 4). All blasted stanchions were at the same time over a height of 15 m correctly destroyed with no plate fly. None of the wall stanchions of the boiler house were to be blasted.

Figure 21. Boiler tilting.

Figure 22. Boiler tilting.

Figure 23. Blast result: boiler debris heap.

6 SUMMARY AND CONCLUSIONS

The blast demolition method ‘water blasting’ can replace other steel blast methods like linear shaped charges or kicking charges in case of hollow stanchions (with a closed cross section). Because this method needs no large pre-weakening it is safer than other methods. Because of the cheaper explosive in regard to linear shaped charges and with an easy realising of high reach blasting zones

the ‘water blasting’ method is cheaper too. The water dust of the blast can help to take down a part of the dust cloud. The new water method has so far been used on 56 steel structure objects in Germany. This number contains 45 large steam boilers in power plants. Hollow objects, constructed of reinforced or pre-stressed concrete, such as bridge pillars or silos are also able to be blasted with this new water method.

REFERENCES

Melzer, R. 2004. Water blasting of hollow steel stanchions; *Sprenginfo, March 2004 (Proceedings of German Blaster´s Society*. Deutscher Sprengverband.

Melzer, R. 2015. New formulas for charge weights in blast demolition. *EFEE 8th World Conference* Lyon 2015.

Stockholm Conference Proceedings 2017, R. Holmberg et al

Blasting close to a substation with a low threshold value. Test blasts, vibration prediction and execution of rock excavations

S. Ahrengart, E. Malmquist & M. Jern
Nitro Consult, Sweden

ABSTRACT: This paper describes a project that was performed in Västerjärva, a suburb of Stockholm. A low threshold value (2 m/s^2) at a nearby electrical substation meant that blasting for new residential buildings became a challenging task. This paper describes how test blasts were performed in the area and how the data from these test blasts was used to make recommendations regarding the excavation of the area. It also describes how the excavation was performed and discusses how accurate the predictions made were in relation to the actual result. The analysis included the charge weight scaling law equation as well as a signature wave superposition model. This was to be able to predict, not only, MIC but also delay time and the influence of blast direction, blast hole screening etc.

1 BACKGROUND

Järvastaden AB is establishing residential buildings in Västerjäva, a suburb 12 km north of Stockholm city centre. Approximately 60,000 m3 rock must be excavated to create the correct level for the buildings. Rock excavations have to be made just 50m from a substation (Figure 1) east of the area with equipment in the form of gas-filled switchgear and circuit breakers. The threshold value for blast-vibrations was set to 2 m/s^2 (by the owner of the substation) which is very conservative.

During the summer of 2013 a contractor initiated rock excavation, but had to stop working when the threshold value for blast-vibrations was exceeded at a distance of nearly 150 meters from the substation. To be able to perform the rock-excavation in the area, Järvastaden AB asked Nitro Consult to perform a pre-study of the area starting with a test blast. During autumn 2014 Nitro Consult performed test blasting to investigate different options for performing full scale blasting in the area.

The aim of the test blast was to investigate the options available for production blasting but also to investigate how close to the substation blasting could be performed. The test blast was also designed to give recommendations for production planning criteria including; drill patterns, delay-times including maximum instantaneous charge (MIC) and excavation planning.

Figure 1. The substation.

2 METHOD

In principle two different methods were used to decide how to excavate the area. After the test blast the data was analysed using regression analysis and the charge weight scaling law equation. In order to further analyse the data a superposition model was used in order to make suggestions regarding delay times and geometry of the blasts.

2.1 The charge weight scaling law equation

The charge weight scaling law equation is the most common method to calculate vibrations from blasting regarding size and distance (through regression analysis). In the Superposition model however, it is just a part of the model, the equation of the charge weight scaling law equation is in this case:

$$v_{\max} = A \cdot \left(\frac{R}{Q} \right)^{-B} \qquad (1)$$

The parameter: $\left(\frac{R}{\sqrt{Q}} \right)$ is often called SD (scaled distance)

Where:

v_{max} = maximum peak particle velocity (mm/s),

R= distance (m)

Q= charge weight (kg)

A= site specific constant

B= site specific constant

(Instead of $v_{max.}$, we can use acceleration (a_{max}) in the same equation to predict acceleration instead of vibration velocity. The A & B parameters will however be different and not correlated).

2.2 The superposition model

The difference between the superposition model and the way vibrations traditionally have been calculated (charge weight scaling law equation) is primarily that the concept of time is introduced into the calculations, and in this way it's possible to optimise the blast after considering different initiation plans.

The model uses Monte Carlo simulations whereby you include variability in governing parameters that cannot be exactly determined (due to geological uncertainties, delay scatter in the initiators etc.) and then you run the model many times in order to quantify a statistical distribution. The model is a waveform superposition model; so that the result is calculated by superposition of several charges which have similar vibration shapes but are different in time and space.

The model was originally developed by Dane Blair and has been described in several publications (Blair 1999, 2004, 2007). It's included in Orica mining services software SHOTPlus Professional. The model has been described more in detail in several papers, among others, Jern 2011.

In the calculations you use a seed wave which gives information about how the vibration changes depending on the medium it travels through between the place of the detonation and the monitoring point. The properties of the seed wave are a 'finger print' that consists of information regarding the geological properties that govern the vibration. The principle of the model is shown in Figure 2.

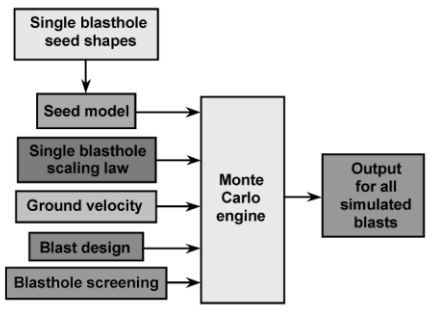

Figure 2. Block diagram of the Monte Carlo model.

Beside the Scale distance equation (and the scatter of raw data) other input to the model includes: Blast design, the Seed wave (the shape of the recorded single hole blast curve), p-wave velocity and blast hole screening.

3 THE TEST BLAST

The test blast was performed with 6 single hole shots (darker number legend) with different charge-weights depending on the distance from the substation, see Table 1. The charge-weights used for the test-blasts were calculated with the experience from earlier blasting that had proceeded in 2013. The main focus was to be able to use a maximum amount of charge to pick up signals in the vibration-monitors but not to exceed the threshold value on the substation.

Holes were drilled in a straight line from the substation. Two holes were drilled at each distance from the substation in order to have the possibility to do a re-shoot. The holes were drilled to 38 mm diameter and between 6.8-7.5 meters deep from the surface.

Vibrations-monitors were mounted at six different places (pale grey number legend), see Figure 3. Three vibration monitors were mounted on the bedrock. Two vibration-monitors were mounted on the substation, one on the foundation on the outside of the building and one on the inside on the concrete floor. These vibration-monitors were tri-axial geophones measuring vibration velocity. One monitor was mounted on the switch-gear with tri-axial accelerometers, see Table 2. Evaluation was done according to SS 460 48 66 (5-300 Hz) for vibrations and according to ISO 8596 (5-300 Hz) for acceleration.

Table 1. Charging-weight in each single-shot and distance to the switch-gear in the substation.

Single - shot	Charge-Weight [kg]	Distance to substation [m]
1	1.987	151
2	0.984	113
3	0.734	82
4	0.489	65
5	0.488	53
6	1.214	83

Table 2. Vibration monitors and distance to the switch-gear in the substation.

Vibration monitor	Type of measure	Distance from sub-station [m]
1, Substation, foundation	Tri-axial, mm/s	3
2, Bedrock	Tri-axial, mm/s	40
3, Bedrock	Tri-axial, mm/s	47
4, Bedrock	Tri-axial, mm/s	69
5, Substation Switch-gear	Tri-axial, m/s²	0
6, Substation floor	Tri-axial, mm/s	1

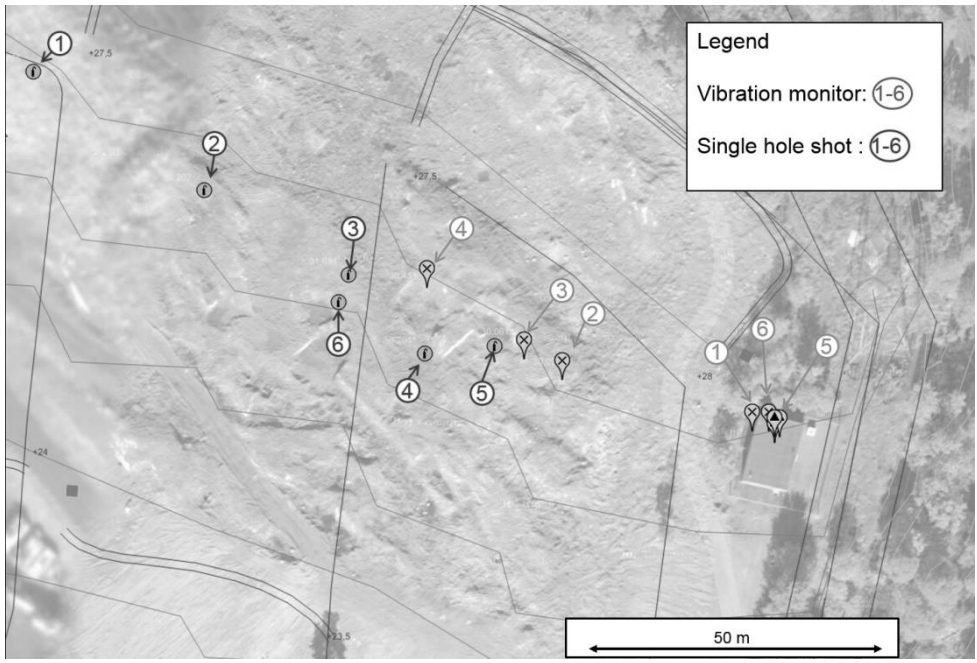

Figure 3. Map presenting 6 single shots (dark legend) and 6 vibration monitors (pale grey numbers). The substation is on the right side of the map.

3.1 Procedure during test-blast

During the test-blast, one single hole shot was fired at a time, beginning with the shot furthest away from the sub-station. The charges were initiated by pyrotechnic detonators, Exel.

After the shot was fired, recorded vibrations were analysed for obtained vibration-level and quality of the signal. After this vibration control was performed, the next hole was charged and fired.

It was observed after shooting hole number 3, that the level of vibrations was very low. A second single-shot was fired, shot number 6, with an increased charging weight, shown in Table 1.

4 RESULT FROM THE TEST BLAST

4.1 Regression analysis

The charge weight scaling law equation is calculated with regard to vibration velocity and acceleration. Since the limit value on the substation was related to acceleration that was the most important value but vibration velocity was also considered. All analysis was done in the vertical direction only in accordance with Swedish praxis, see Figures 4 and 5.

4.1.1 Charge table – regression analysis

The regression line from Figure 4 and the following model parameters (Table 3), enabled us to create a charge table (Table 4). Knowing we have to remain below 0.2 g (2 m/s^2) and by using a probability of 84% (1 standard deviation), we can use a 0.75 kg charge at a distance of 50 m. However since the substation gives lower acceleration values (Figure 4) than the surrounding monitoring points the results table will likely be disappointingly low. Due to this fact it was decided to repeat the analysis using vibration velocity instead.

Figure 5 shows that the recorded values at the substation fit better with the other measurements for vibration velocity than the observations of acceleration (although the overall fit isn't as good). An explanation for this can be seen in Figure 6. The frequency is generally lower (and very constant) for the substation than for the monitors placed on rock.

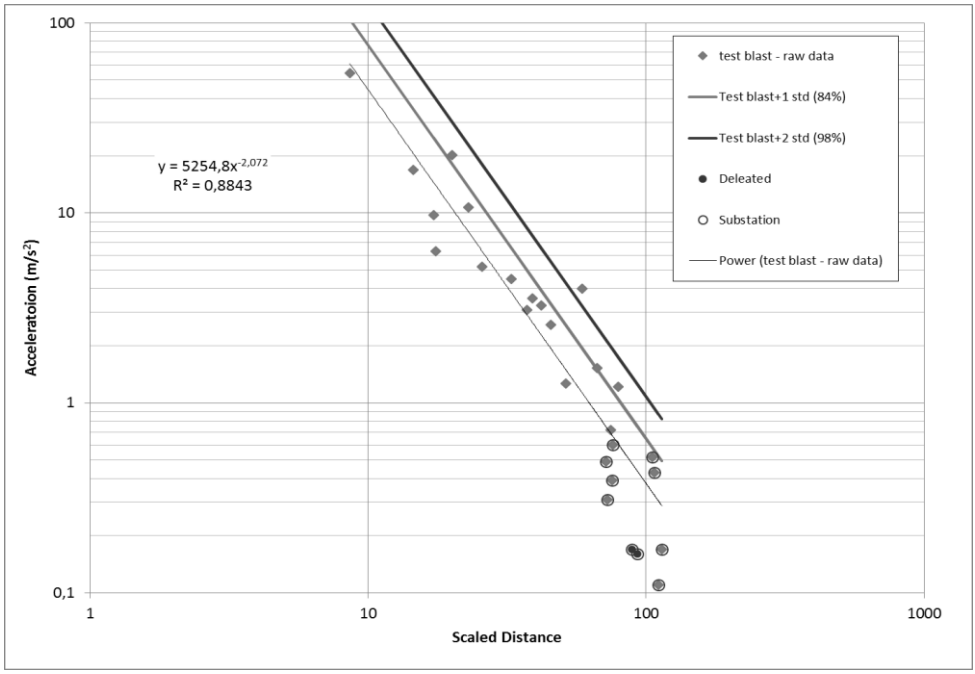

Figure 4. Regression analysis, acceleration.

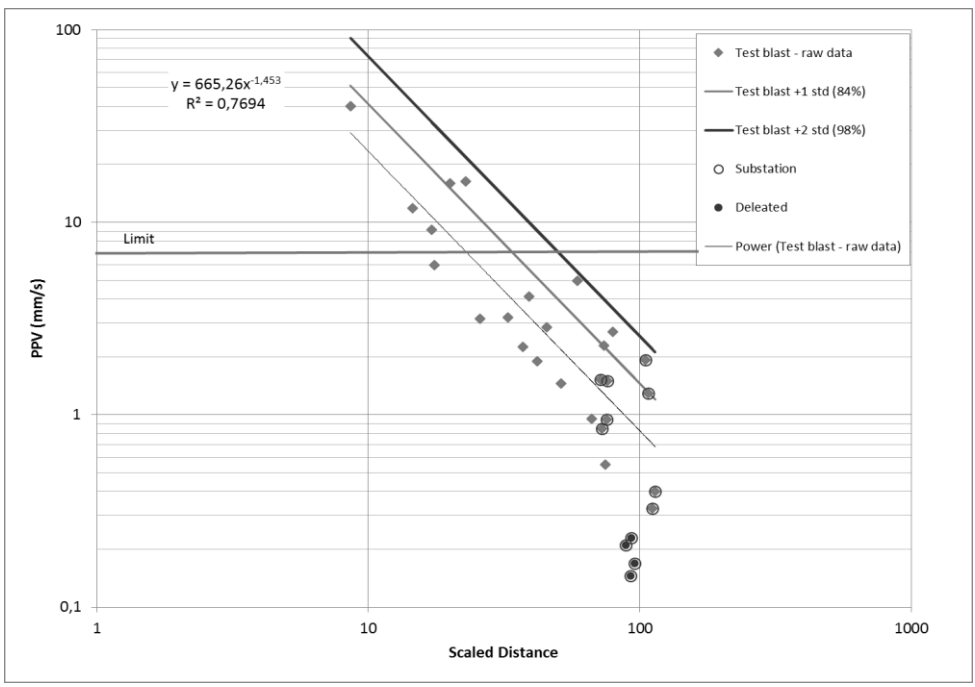

Figure 5. Regression analysis, vibration velocity.

Table 3. Parameters in the model.

	MP
A	655
B	-1.45
vp*	5000
COV**	0.4

*Assumed value
**Coefficient of variation (regarding raw data scatter)

Table 4. Charge table constructed according to model parameters.

R (m)	Q (kg)	50% (m/s2)	84% (m/s2)	98% (m/s2)
10	0,03	1,2	2,0	3,4
20	0,12	1,2	2,0	3,4
30	0,27	1,2	2,0	3,4
40	0,47	1,2	2,0	3,3
50	0,75	1,2	2,0	3,4
60	1,05	1,1	2,0	3,3
70	1,45	1,2	2,0	3,3
80	1,9	1,2	2,0	3,3
90	2,4	1,2	2,0	3,3
100	3	1,2	2,0	3,4

It can be seen that the dominating frequency at the substation was around 50 Hz (Figure 6), independent of the distance from the detonation. We can then use the relationship:

$$a = v \cdot 2\pi f \quad (2)$$

If the permissible acceleration level is 2 m/s^2 and the frequency is 50 Hz this gives a permissible vibration level of 6.4 mm/s. Table 5 shows the charge table according to this relationship.

The result of this calculation is that we can charge 3 times as much, 2.3 kg at a distance of 50

Table 5. Charge table for 6.4 mm/s as limit vibration level.

r	Q	SD	50%	84%	98%
10	0.07	37.79645	3.4	6.0	10.5
20	0.36	33.33333	3.7	6.3	10.5
30	0.8	33.54102	3.6	6.2	10.4
40	1.4	33.80617	3.6	6.1	10.2
50	2.3	32.96902	3.8	6.4	10.7
60	3.3	33.02891	3.7	6.4	10.7
70	4.5	32.99832	3.8	6.4	10.7
80	5.8	33.21819	3.7	6.3	10.6
90	7.5	32.86335	3.8	6.5	10.8
100	9	33.33333	3.7	6.3	10.5

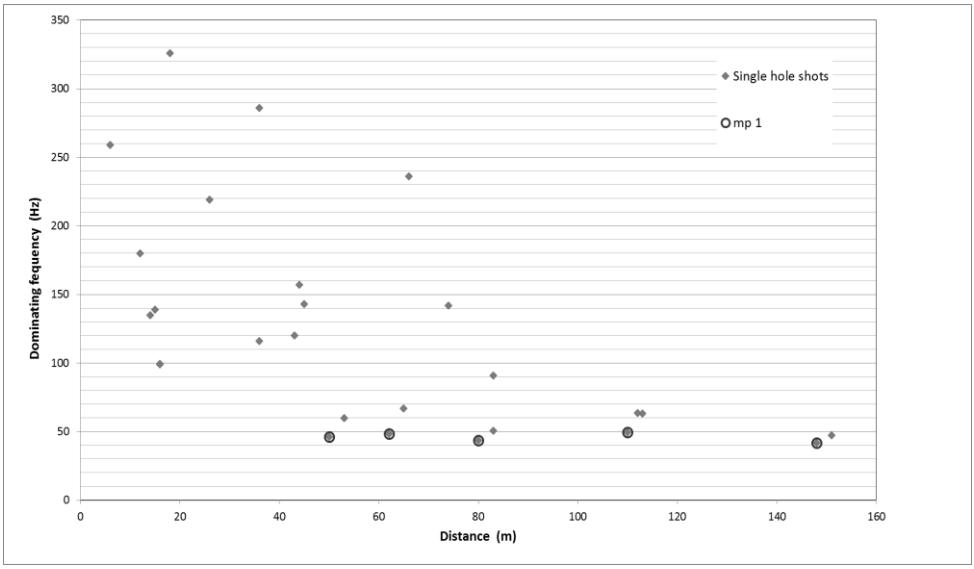

Figure 6. Dominating frequency verses distance, the dark circles come from MP1 at the substation.

Figure 7. Example of three single hole curves, MP 1.

m. The reason for this being, the acceleration levels are generally lower at the substation compared to the other monitoring points on the rock. The underlying difference being that the substation is likely not built entirely on rock and that a thin layer of soft soil reduces the frequencies at the substation.

In general the vibration levels are lower at the sub-station but even more so when it comes to recorded acceleration. This has a big impact on our final recommendations.

4.2 The Seed wave

It is critical that the signature wave form is monitored at exactly the same spot as the modelling will be performed at, this is due to the fact that the wave form is highly affected by how far the wave travels between place of monitor and place for detonation and also due to the response in the constructions monitored.

A condition in order to be able to use the signature wave form is that each blast hole in the modelled blast is similar to the seed hole. In Figure 7 an example of three different signature waveforms monitored at the same spot (MP 1) are shown. What we can see is that the three curves are similar both regarding duration and dominating frequencies. However, you can see that they are not identical, in the model a certain amount of randomisation is introduced to the seed wave form in order to compensate for this variation.

In the simulation made for this project the same seed waves has been used for all distances, it is important to note that the risk of errors increases when the difference between that simulated blast and the original distance for the seed wave increases.

5 USING THE MODEL

Data from the single hole shots were used as inputs to the simulated blasts, the parameters in Table 6 were used, together with the seed wave. This enabled us to decide upon the optimal delay times.

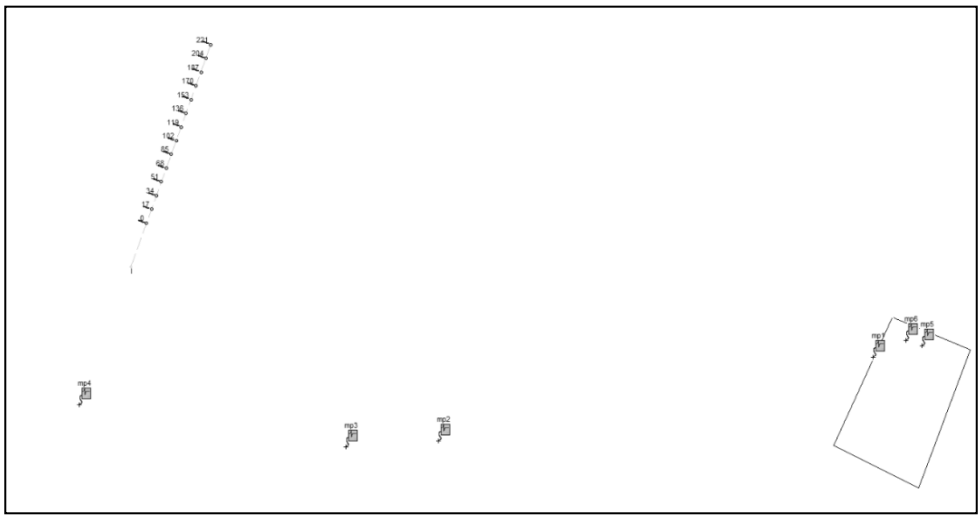

Figure 8. A single row blast at 60 m distance from MP 1, this setting was used to optimise the delay time.

Table 6. Parameters in the model.

	MP
A	655
B	-1.45
vp*	5000
COV**	0.4

*Assumed value
**Coefficient of variation (regarding raw data scatter)

A simple blast was then simulated, 1 row, 14 holes 3 kg of explosive in each hole (see Figure 8 and 9). This blast was simulated with different delay times (from 1 ms to 60 ms, electronic detonators, see Figure 10).

The result from modelling different delay times can be seen in Figure 10. The recommendation from this was to use delay times between 15 and 18 ms, 29 to 42 ms or greater than 45 ms. It was likewise important to avoid using delay times of less than 5 ms and between 19-27ms.

5.1 Recommendations for excavation

The recommendation for excavation was to start by blasting a 'wide trench' from south to north according to Figures 11 and 12 called zone 1. By doing so, the first part of the excavation would create a buffer zone for vibrations from any subsequent blasts in the project and possibly enable the use of a higher MIC.

It was also important to start each blast at the side towards the substation in order to create a buffer zone within the actual blast.

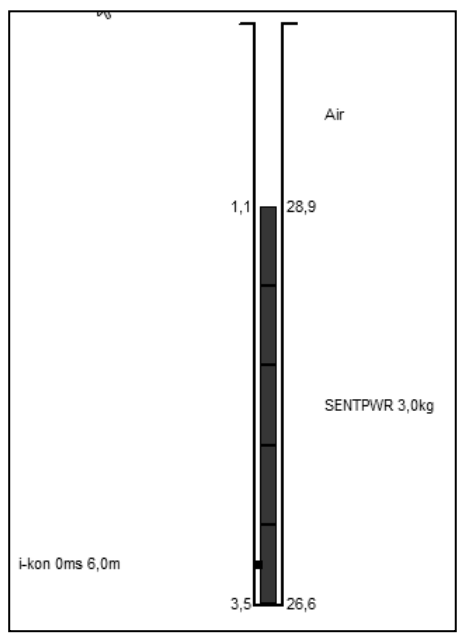

Figure 9. Charged bore hole, 3 kg charge, 3.5 m depth.

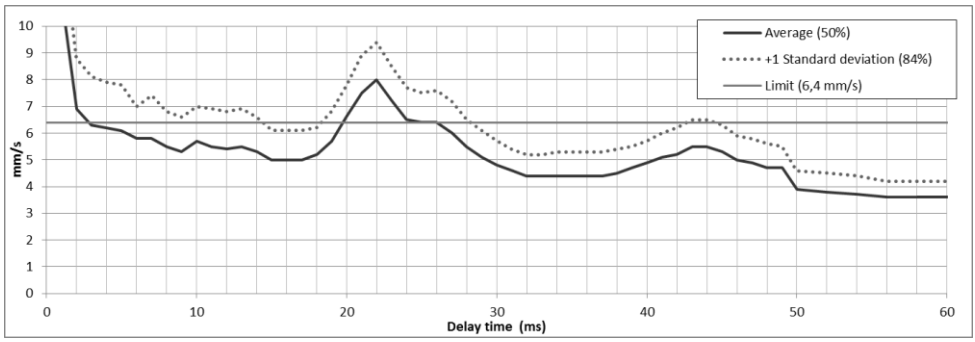

Figure 10. Delay times 0-60 ms between holes.

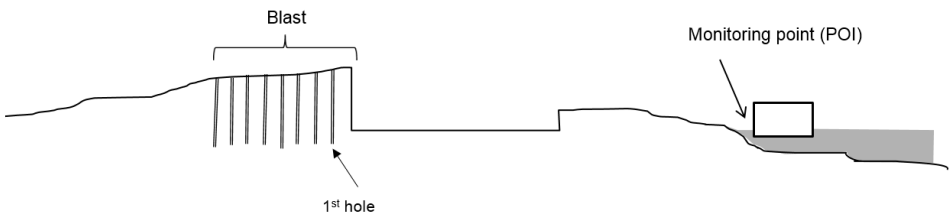

Figure 11. Cross-section of the excavation plan.

From this plan it is possible to test different blasts according to the superposition model. Three different distances 50, 75 and 100 m were modelled according to Figure 13. The condition here was that the level 6.4 mm/s (corresponding to 0.2 g) was a maximum value.

The prognosis showed that it ought to be possible to use 10 kg MIC at 100 m distance. However, a few facts contradicted this. These included: when the earlier project in 2013 exceeded the allowed values the distance was 150 m and the MIC was 5.4 kg and secondly; during test blast 1 at 148 m distance the values at the substation were much higher than during the other test shots.

Due to this it was decided to recommend the usage of a maximum 5.8 kg MIC (burden×spacing then became 1.6×2 m, which would work fine in bench heights up to approximately 5 m).

If the 'wide trench' (zone 1) closest to the substation was shot first the possibility to increase the MIC after that could be evaluated at a later stage.

So blasting was thus planned to start at 50 m distance from the substation (closer than that would have been problematic, due to the small charges involved), blasting from south to north.

6 PRODUCTION

In November 2016 the production contractor, Gnesta Bergbyggare AB started production with blasts in Zone 1. They then made a drill and blast plan with charging and delay times according to the recommendations from the pre-study. Table 7 shows the given MIC and proposed drilling pattern based on the pre-study.

6.1 Procedure development for production blasting

The first design of the production blast were done according to the recommendations from the pre-study.

Before the first blast the real tie-up was modelled in the SHOTPlus signature wave super-position model to simulate expected vibrations.

Figure 12. View over the zones. Excavation starts in zone 1, the zone closest to the substation (MP 6).

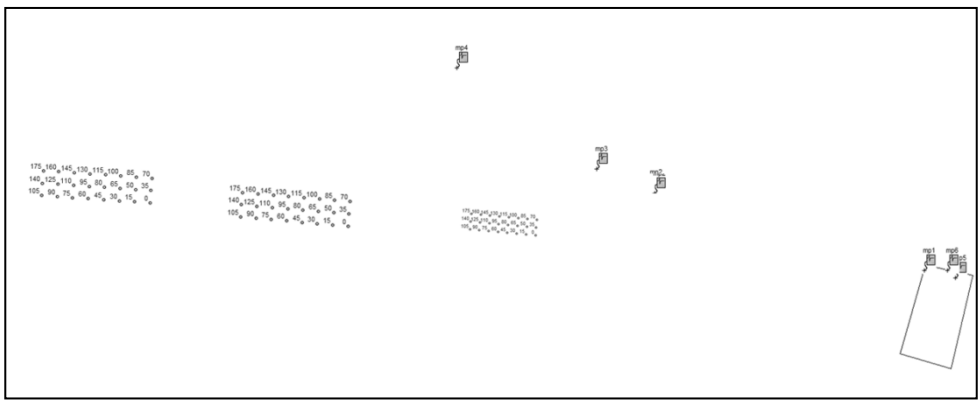

Figure 13. Simulated blasts at 50, 75 and 100 m distance from the substation.

Then immediately before the blast, the initiation plan was marked on the rock to be excavated and noted on paper, (see Figure 14). All holes throughout the blast were initiated by unitronic electronic detonators which make it possible to choose a specific delay time for each hole and ensure only one detonator detonates for each delay time. Having the ability to adjust the blasting plan to reduce vibration levels was an important part of the production procedure. Coordinates for the blast were documented together with the charge load for each detonator and delay time.

Hole-depth, water, difficulties with the drilling and geological aspects were also noted.

After the first blast was fired, monitored vibrations were analysed with regard to all parameters of the vibrations-level including the waveform. By looking at the waveform and the time of the peak-values the specific holes and charges for the peaks were determined.

Table 7. Drilling pattern and MIC for different distances to the substation.

Zone	Distance to substation [m]	Drilling pattern, BxS (m)	MIC (kg)
1	50-75	1.0 x 1.2	2
2	75-100	1.65 x 2.05	4.5
3	>100	1.65 x 2.05	6

Figure 14. The numbers of detonators for that hole together with the charge for lower deck.

6.2 Production blasting

The blasting started in the zone closest to the substation, zone 1, at a distance of 50-75 m away from it. The maximum charge was limited to 2 kg throughout the whole zone. The drilling pattern had a burden and spacing of 1x1.2 m.

The first production blast was located 81 m from the substation and consisted of 21 holes, drilled at a diameter of Ø 48 mm and dipping 10˚ off vertical. The total length of the holes were 0.8-1.2 m. Maximum charge per delay time and hole was 300 grams. The tie-up was made with a 15 ms delay time between each hole. The blast resulted in a vibration value of 0.33 m/s^2 for the substation.

After ten successful production blasts, a higher bench with deck charges was simulated in SHOT-Plus to estimate if the vibration level would stay low, which it appeared to do in the results. The 11th production blast was the first to consist of deck charges, located 76 metres off the substation. Total length of these holes was 3.2-5 metres and had a charge per delay of 1.3-1.8 kg. The blast resulted in a vibration value of 0.67 m/s^2 .

Zone 1 was then divided in two zones with a maximum bench height of 6.5 metres, to make it possible to blast one full bench height with two decks. The top bench was carried out for the entire zone before production started on the bottom bench.

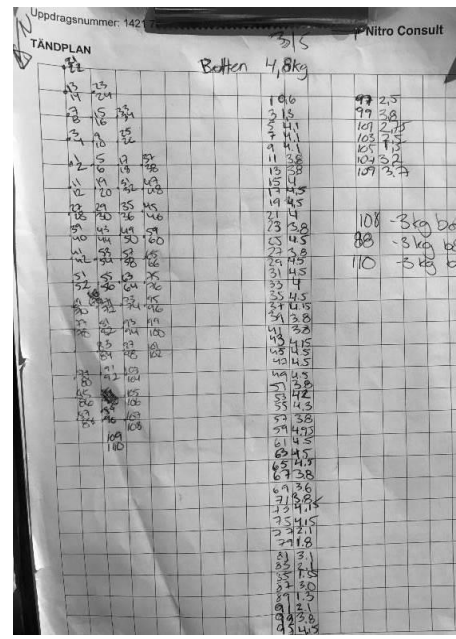

Figure 15. The documented tie-up together with all charges for the blast.

6.3 Production blasting improvements

The success of blasting higher benches and maintaining low vibration values made it possible to try even bigger production blasts. This even meant sometimes as production got closer to the substation the blasts got bigger. The key learning

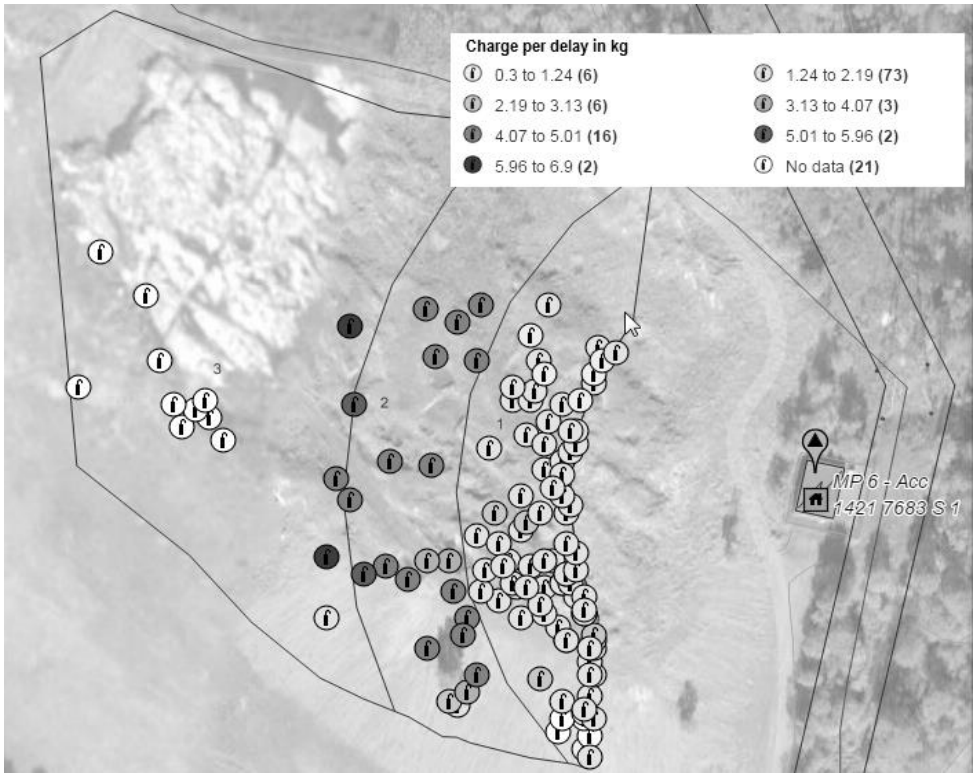

Figure 16. Location of the 120 production blasts. Charge per delay are shown in greyscale according to the legend in the figure.

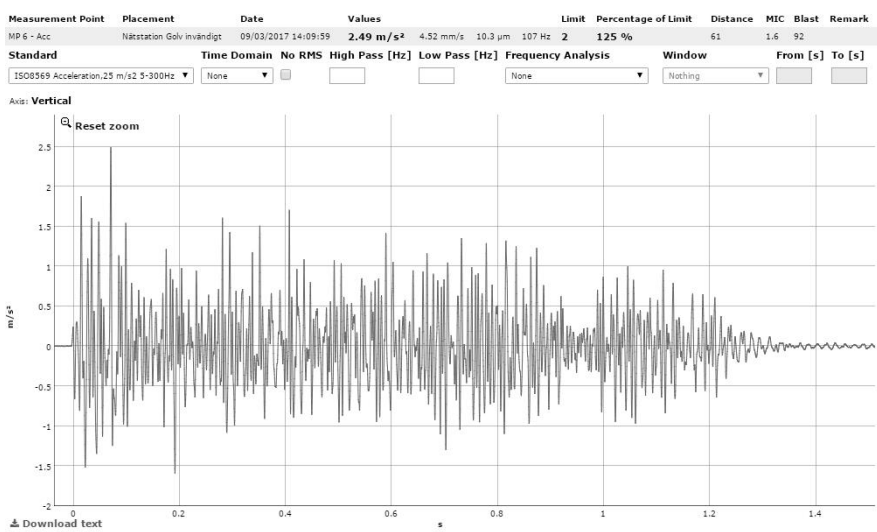

Figure 17. Waveform of the acceleration from blast 92.

being, when we approached the 50m limit to the substation, the two rows closest to it only got charged with a maximum of 1.5 kg to ensure low vibrations.

The biggest production blast in zone 1, consisted of 98 holes, 480 m^3, charged with a total of 240 kg over two decks. This blast included 193 detonators initiated with a 15ms delay time and a maximum charge of 2 kg per delay. The blast resulted in an acceptable vibration value of 1.5 m/s^2.

These larger production blasts sometimes resulted in undetonated explosives and big blocks at the surface. To eliminate undetonated explosives and achieve better fragmentation and heave from blasting the idea of using shorter delay times was proposed. A subsequent initiation plan was run in SHOTPlus where the delay time was lowered from 15 ms to 7 ms without increasing vibration values. The 7 ms delay time was then used as the new standard for further blasting and the amount of undetonated explosives appeared to decrease.

In the beginning of May 2017, 120 blasts had been made in the area at distances between 50 – 160 m from the substation. Figure 16 shows charge per delay for all blasts.

The only exceedance of the threshold value occurred during blast 92 in April, 2017. This exceedance resulted in a few days stop in production while the waveform and vibration values of the blast were analysed. The key aspect of the analysis being to determine the reason for the high acceleration. Figure 17 shows that there was only one peak that exceeded the threshold value of 2.0 m/s^2. The delay time and specific hole could be estimated by looking at the documented tie-up for the blast.

The frequency for the top value was around 60 Hz and Figure 16 shows PPV and PPA for all 120 blast monitored before May 2017. If the relationship between acceleration had been strictly linear (according to the relationship used when calculating the MIC), the acceleration would be around 1.7m/s^2. We believe the geology in that area probably contributed to the exceedance.

When blasting resumed the new MIC for the two rows closest to the substation was decreased to 1 kg. The rest of the blast got charged the same way as earlier blasts in the same zone.

7 DISCUSSION

In general the project can be seen as a success.

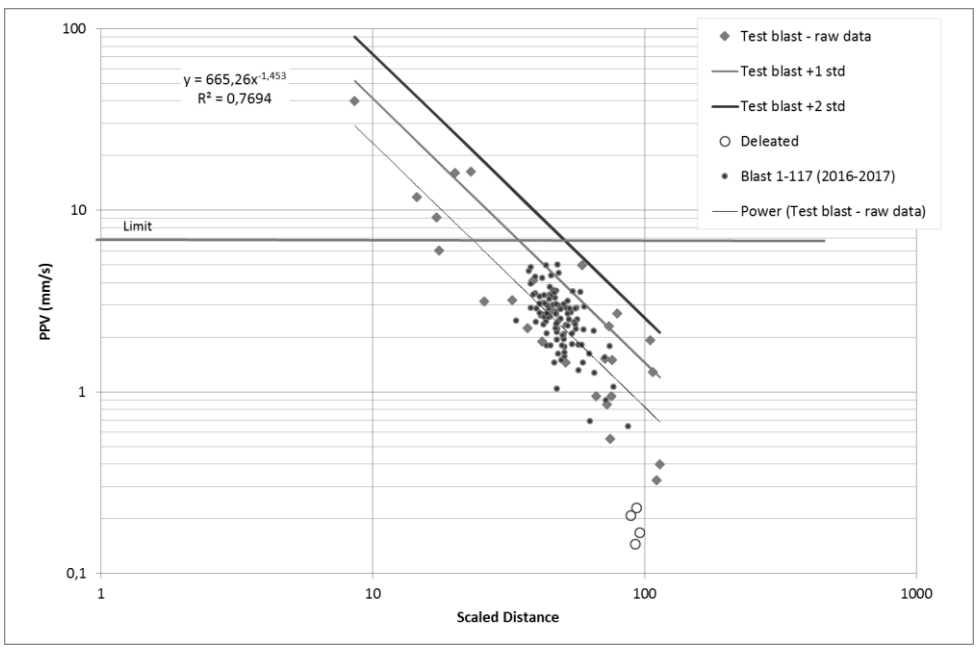

Figure 18. Good agreement with the PPV prediction.

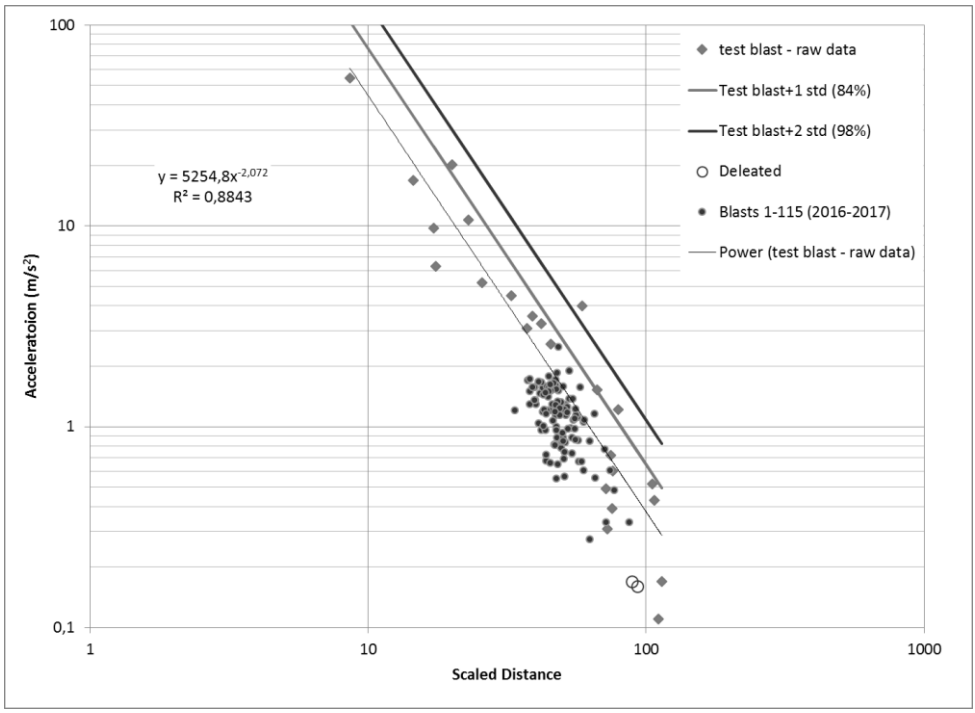

Figure 19. The acceleration levels plot low in the diagram.

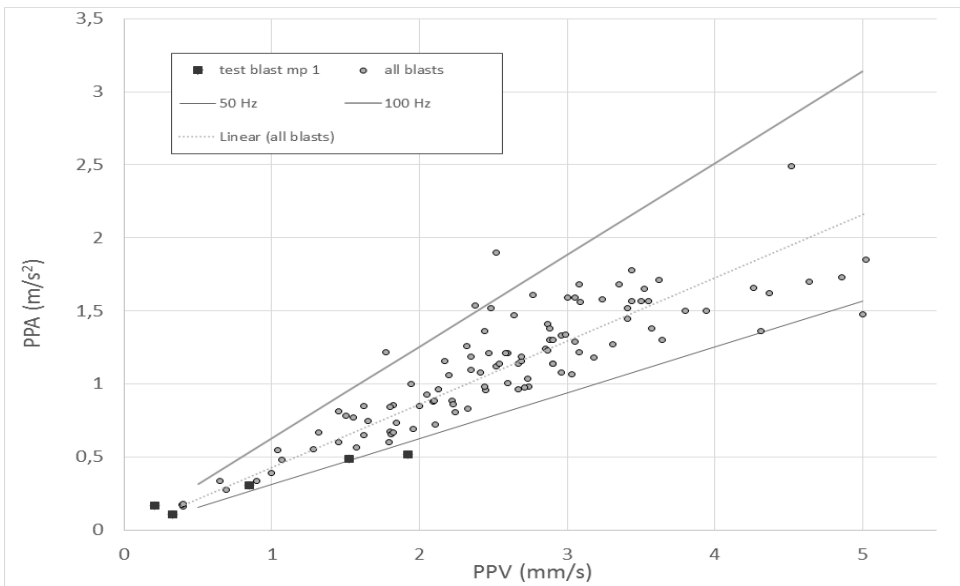

Figure 20. The relation between PPV and PPA. The lowest line shows the predicted line (50 Hz) corresponding to the test blast (dark squares), while it can be seen that the actual relation between PPV and PPA varies between 50 and 100 HZ averaging at 67 Hz (the dotted line).

Only one of 120 blasts has recorded a vibration level above the threshold at the substation. Comparing the production blasts with the single hole shots we can see that the correlation is good. This can be seen in Figures 18 and 19 where we have plotted the individual blasts in the same diagram as the regression analysis for the single hole blasts. What we can see is exactly as predicted the results are in good agreement with the PPV prediction (Figure 18) while the acceleration levels plot low in the diagram (Figure 19).

We can also note that although some blasts have been large with almost 200 separate charges it has been possible to keep the vibrations at the same level as the one single hole shots.

The reason why the threshold level (2 m/s^2) was exceeded one time (Blast# 92), despite the calculated threshold level (6.4 mm/s) never been breached, was that the acceleration level had been higher than predicted and the reason for that was that the dominating frequencies were higher than the predicted 50 Hz, not only in that blast, but in most blasts.

The spread in dominating frequency between the different blasts were large and as a result it was difficult to establish a clear reason. The average dominating frequency for all data (using the relation $a=v\times 2\pi f$) was 67 Hz, leading us to believe that this was due to the 15 ms delay time (1/0.015 s =) 67 Hz. However when we looked more closely at the data we noticed that also blasts with a 7 ms delay had an average frequency of 67 Hz, informing us that differences were in fact due to how the blasts were shot.

Due to the size of the allowed MIC (2 kg), zone 1 had to be divided into 2 benches (where each bench was shot with 2 decks). If we compare these 2 benches we can see that the acceleration values were higher in the lower bench and this appears valid by just looking at the 7 ms delay times. However the understanding that the acceleration (frequency) is higher than the predicted 50 Hz being solely dependent on an effect from the delay timing is not accurate. Another reason is that when the lower bench was being excavated this gave an even higher frequency due to an improved contact (for wavelengths to propagate) between the lower bench rock and the substation than for the upper bench, see Figure 21.

8 FINAL CONCLUSIONS

In conclusion, the recommendations put forth

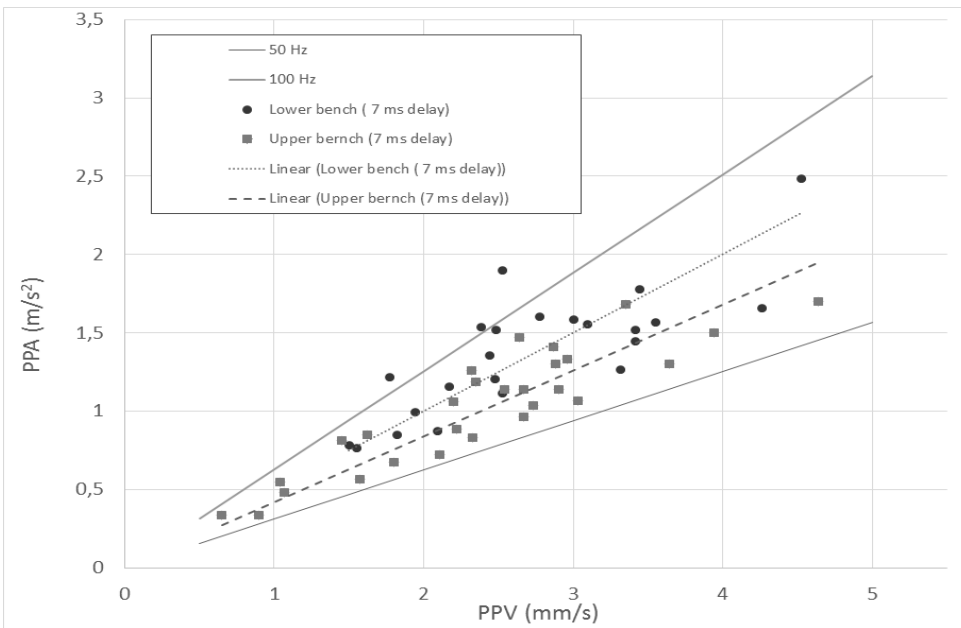

Figure 21. The relation between PPV and PPA. For just the 7 ms delay shot. The upper bench (dark squares) gives an average frequency of 67 Hz while the lower bench (black circles) gives 80 Hz.

regarding vibration velocity have worked well in this project.

In all, out of 120 blasts that were recorded in the project the vibrations have been within acceptable limits every time except once. The superposition model, our recommendations and the possibility to include delay timing has been very helpful in ensuring this occurred.

The ultimate indicator and success of the method being that, we are able to produce large blasts consisting of a large number of holes with two decks while still succeeding to keep the vibrations on the same level as the single hole shots. This being largely due to the contribution of electronic detonators and the possibility to calculate optimal delay times.

The observed accelerating values were higher than predicted due to the driving frequencies from the delay time of the detonators, this was not properly included in the initial predictions. Thankfully, the consequence of this was minor and not a limiting factor to the success of the project.

REFERENCES

Anderson, D.A. 2008. Signature hole blast vibration control – twenty years hence and beyond. *Proc of the annual conf. of explosives and blasting technique*. V 34(2): 27-38.

Blair, D.P. 1999. Statistical models for ground vibration and airblast. *Fragblast, The International Journal for Blasting and Fragmentation*. V 3: 335-364.

Blair, D.P. 2004. Charge weight scaling laws and the superposition of blast vibration waves, *Fragblast, The International Journal for Blasting and Fragmentation*. V 8: 221 – 239.

Blair, D.P. 2007. Non-linear superposition models of blast vibration. *Int. J. of Rock Mechanics and Mining Sciences.* V 45: 235-247.

Jern M. 2011 Test blast and vibration prediction AVM project Klinthagen Quarry, Gotland, Sweden. *Proc. of the 6th conf. on Explosives and Blasting*. Lisbon Portugal EFEE pp 91-116.

Spathis, A.T. 2009. A brief review of the measurement, modelling and management of vibrations produced by blasting. Workshop on vibrations from blasting 12-13 September 2009 Granada, SPAIN: 1-11.

ISO 8569:1996. Mechanical vibration and shock -- Measurement and evaluation of shock and vibration effects on sensitive equipment in buildings.

SS 460 4866:2011 Swedish Standard SS 460 48 66 Vibration and shock – Guidance levels for blasting induced vibration in buildings.

Stockholm Conference Proceedings 2017, R. Holmberg et al

600,000 MT to move, a high-risk operation

J-S. Lambert
Protekroc Inc, Quebec, Canada

ABSTRACT: At the end of 2014, Holcim Canada considered the possibility of drilling and blasting a big volume of rock in order to expose a high-quality limestone bench in one of their urban-area quarries in Laval, Quebec (Canada). The project includes many challenges and has thus been qualified as a high-risk operation. Due to the extraordinary size of the urban blast, the company Protekroc, a drilling and blasting engineering firm, was commissioned to design the geometry of these blasts and establish the process of control needed to achieve the desired results with the respect to the environment and the standards set by the owner. To achieve the goals: i.e. the control of the projections, the control of the vibration, control of the air overpressure and the fragmentation results, Protekroc conducted a comprehensive and detailed analysis of each stage of the project in order to determine the appropriate procedures.

1 INTRODUCTION

At the end of 2014, Demix Aggregates considered getting a significant amount of limestone. To achieve their goal, the possibility to realise two big blasts must be analysed. The stone volume going to be excavated is located at the south-east limit of the quarry neighbouring Boulevard St-Martin and several shops and residences. In order to get the greatest possible volume of stone, the blast must be shot on a single bench with a height of about 24 m. The blasting process will be divided in two steps. The site for the first blast estimated at about 375,000 MT, is the east wall of the proposed excavation. The second blast will be about 220,000 MT.

Figure 1. General view.

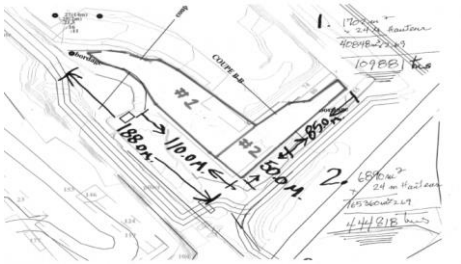

Figure 2. Initial sketch.

2 MANDATE

Due to the extraordinary size of the urban blast, the drilling and blasting consultant was commissioned to design the geometry of these blasts and to establish control necessary to achieve the desired results with respect to the environment and the standards set by the owner. The main goals were the control of the projection, the vibration control, the control of the air overpressure and the expansion of the heap allowing the facilitation of the excavation. Several buildings are located within a radius of 350 m (1,148 ft); they are likely to be affected by the two blasts. The proposed control measures take into account the environment around the blast site. The drilling and blasting consultant conducted a comprehensive and detailed analysis of each stage of the project in order to determine the appropriate procedures as well as the drilling and blasting parameters.

3 POST BLASTING RECORDS CHECK-UP

To correctly identify the methods used and the results achieved historically in the quarry of Laval, several blasts having been shot in the same area were used to assess the site response. The vibrations produced and the shape of the blast obtained were compiled together in order to calibrate the model.

4 GEOLOGICAL AND SITE ANALYSIS

The first visit to the site was conducted on 11 December 2014. A geologist and a senior mining

Figure 3. Aerial view.

and RM specialist made an assessment of the site. The vibration, the air pressure, the projections of rocks and the stability of the high walls were the main concerns.

The report points out the low risk of limestone blocks reversal with joints parallel along their plane of weakness. In addition, it mentions that the joints found in blasting areas are not a big risk against the planned blasting. According to the main concerns, the following actions were undertaken: a signature holes campaign, a pre-blast inspection survey, a dialogue with the neighbours, a planification of a pre-shear along the final wall before the mass blast.

Figure 4. Site condition (December 2014).

5 SITE SURVEY

Several scans of the existing walls were conducted due to the changing conditions on the site; we had to clean the bench of the melting snow and excavate loose material. The grid used for the survey was 0.3 m by 0.3 m (1 ft by 1 ft).

Figure 5. Blast #1.

6 GEOMECHANICAL PARAMETERS

Some physical tests were made on rock cores. A summary of the results obtained during the tests are presented in table 1.

7 SIGNATURE HOLES

A signature holes analysis was conducted on 26 January 2015. The purpose of this measure is to determine the seismic signal produced by a single hole at a particular point outside shooting. This seismic signal was used in I-Blast to simulated the vibration and optimise the timing. The positioning of the seismic stations was determined with regard to the infrastructure to be protected.

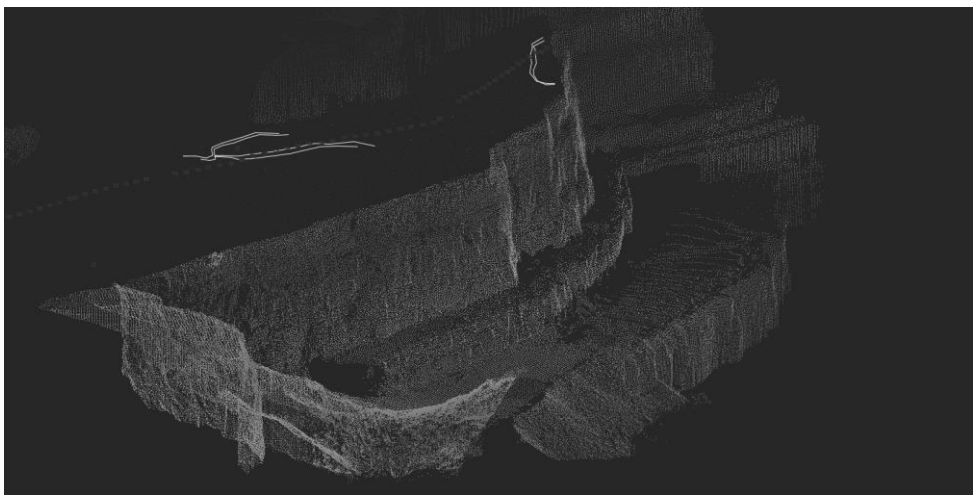

Figure 6. 3D model.

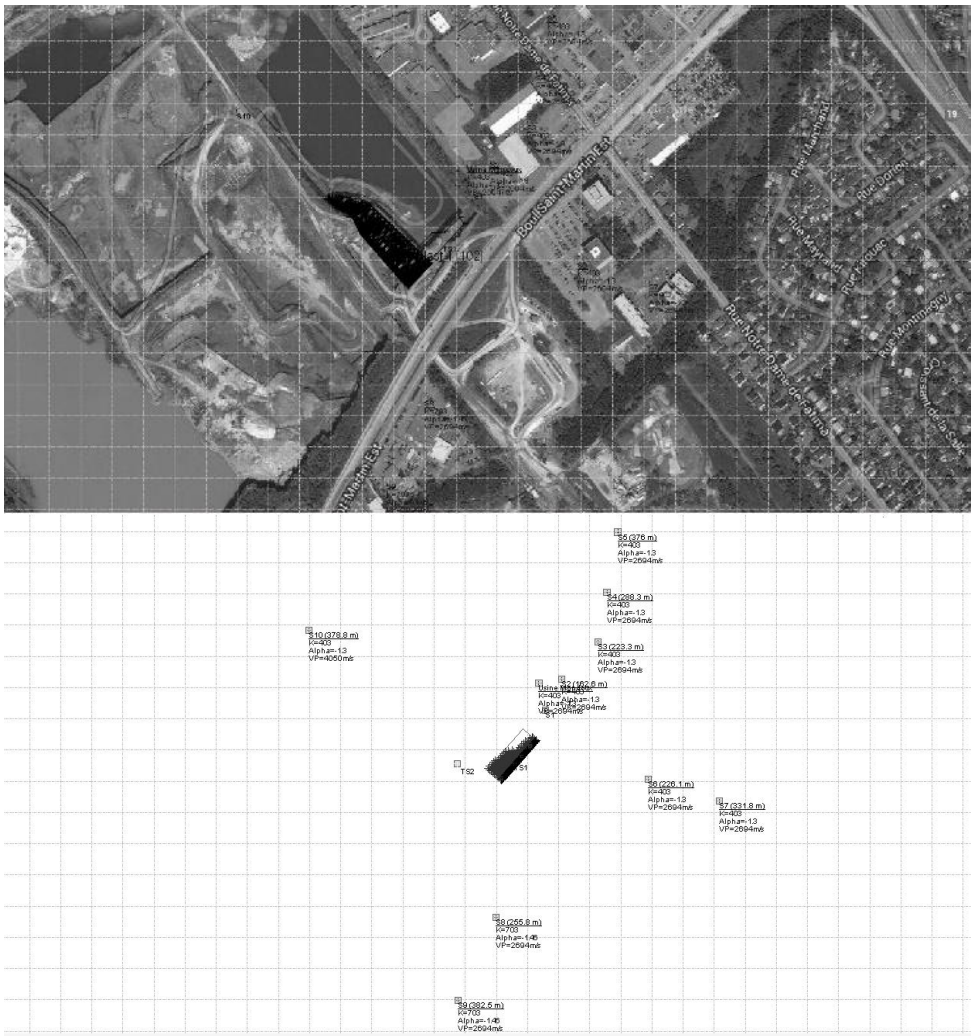

Figure 7. Signature hole seismic stations and measured parameters.

Table 1. Geomechanical parameters calculated.

#	Trials	Individual Results				Average
1	Compressive strength (Mpa)	86.70	110.70	76.30	91.20	91.20
2	Tensile strength (Brasil) (Mpa)	7.20	3.10	5.20	5.20	5.20
3	Elasticity module (Gpa)	43.40	38.10	21	34.20	34.20
4	Poisson coefficient	0.19	0.16		0.18	0.18
5	Particule density (SSS)	2.692	2.741	2.68	2.704	2.704
6	Absorption	0.80	0.21	0.37	0.46	0.46

Figure 8. Seismograph installation

8 ATTENUATION LAW

The measures taken in the field have enabled us to establish the following attenuation laws.

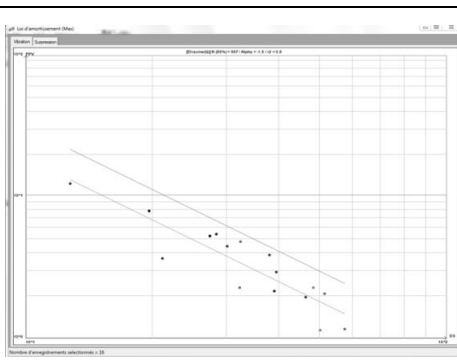

Figure 9. Attenuation law.

The result obtained after the treatment of our two signature holes was remarkable. Due to the quality of the readings acquired, we were able to accurately define the values of the terrain parameters, i.e. the 'K' and the 'alpha'. Note, that according to the results obtained, these parameters vary depending on the exact zone. Zones 1 to 6 show the same behaviour, a 'K' of 430 and an 'alpha' of 1.3 while zones 7 to 10 have a 'K' of 887 and an 'alpha' of 1.46. The correlation for these two cases was respectively 0.98 and 0.80.

9 PARTICULAR VELOCITY

During our signature holes study, measures have been taken to determine the speed of particles (Vp). Two methods were used for this purpose; one being the use of a wire trigger installed on a Micromate. The second method includes the use of an electronic detonator triggering the microphone of another Instantel sismograph. Following the analysis of these results and their interpretation, we used a Vp of 4,664 m/s (15,301 ft/s).

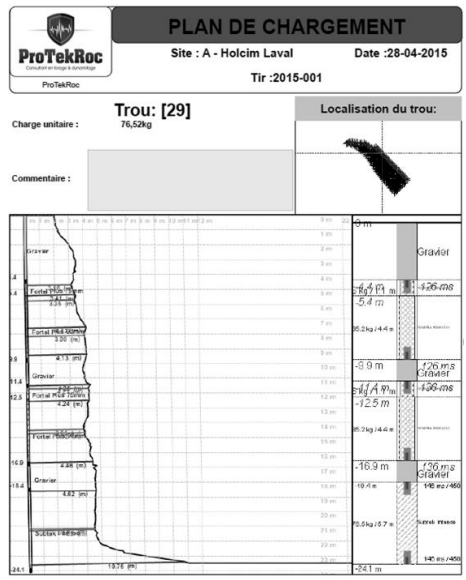

Figure 10. Face profile example

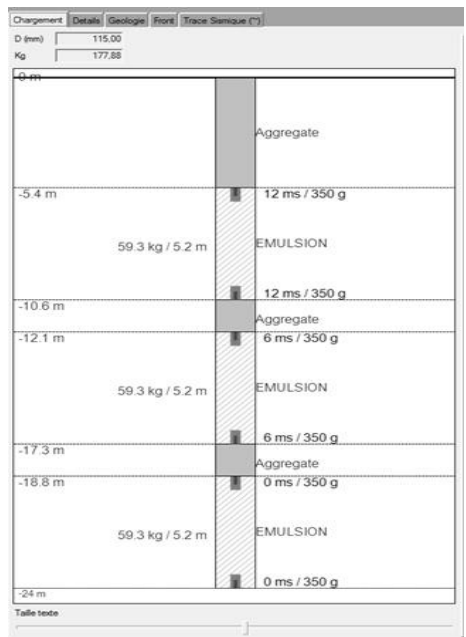

Figure 11. Typical loading.

Figure 12. Emulsion used.

10 BLAST DESIGN

The data collected allowed us to establish the parameters of the geometry of the upcoming blast. All the drilling and blasting parameters were analysed and defined according to the main goals and concerns. A diameter of 115 mm (4.5 in) was finally chosen. The pattern was 3.5 m (11.5 ft) by 4.5 m (14.8 ft) with a bench height of approximately 25 m (82 ft). The explosive used in the production hole was a doped emulsion, the subtek Intense from Orica. With the smart loading function of Thierry Bernard Technologie software, we were able to determine the maximum charge allowed for each hole. The powder factor used was about 0.60 kg/m^3 (0.78 lbs/yd^3). Due to the size of the blast site, the surrounding conditions and the vibration control challenges, electronic detonators (I-kon from Orica) were used. A stemming plug was utilised in order to increase the performance of the collars. Each exact profile for every hole of the first row was drawn using the scan survey data and the profile of the hole measured with the probe. Each loading was updated in accordance with the minimum burden fixed in relation with the diameter of the explosive. The pre-shear was done with the help of a 32 mm (1.25 in) continuous packaged explosive. Fine sand and geotextile were placed on top of the holes to minimise air-blast and projection.

11 TIMING

The timing was determined with the signature holes method with the help of I-Blast Software. The calculation was based on the signature holes study made at the end of January 2015. The optimum delay between two holes was 28 ms and the optimum delay between decks was 7 ms. These values allowed us to use 3 decks per holes.

Figure 13. Pre-shear protection.

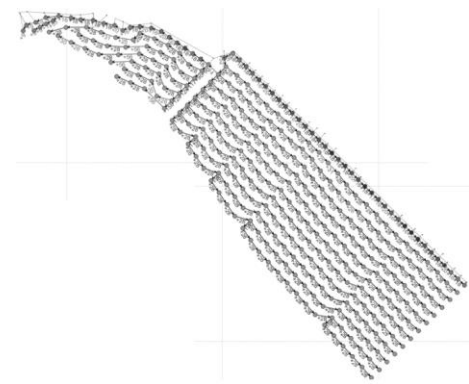

Figure 14. Connection plan.

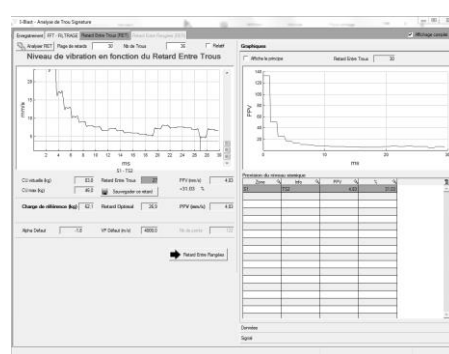

Figure 15. Signature hole analysis.

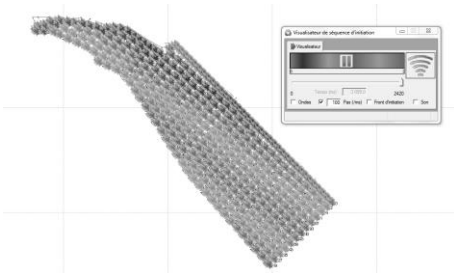

Figure 16. Sequence analysis.

12 DRILLING

To make sure we had the energy at the right place, we introduced different controls. Every hole was positioned by the GPS, the precision of the drilling was checked with a probe, the depth of the hole was checked and adjusted, if necessary. The drilling was made with a top hammer drill equipped with a retract-type bit, guide steel and a 60 mm (2.34 in) rod. Every abnormality had to be reported in the drilling log to allow the loading adjustment, if necessary. A total of 552 holes were drilled. The deviation profiling campaign was made on over 120 holes, mainly on the holes from the first and the second row and the pre-shear holes. More than 50% of the holes were under 2% of deviation. 8 holes in total had to be re-drilled.

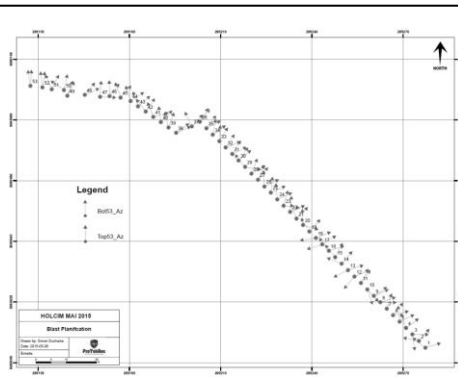

Figure 17. Deviation analysis tool.

13 WORK INSTRUCTION

Every parameter, established during the design, was verified, measured and controlled. Work instructions were created according to the design, which explained the sequence of the stages of operation and enumerated the associated control measures.

Figure 18. Deviation control operation.

14 ZONE OF CLEARANCE

A zone of 100 m (328 ft) around the blast site was totally evacuated. The zone between 100 m (328 ft) and 200 m (656 ft) from the blast point had to be cleared of the public.

15 SIMULATION

The Mines and Quarries Regulations limits to 40 mm/s (1.57 in/s) the particle velocity measured near the structures to be protected. The design of the blast was made in respect of the limit established by the owner of 12.7 mm/s (0.5 in/s). Simulations were carried out to confirm the vibrations level at the zones to be protected. Simulations on projections were also performed to confirm the size of the clearance zone. The air overpressure was also simulated under various conditions.

16 LOADING OPERATION

The blast occurred on Saturday, 16 May 2015.

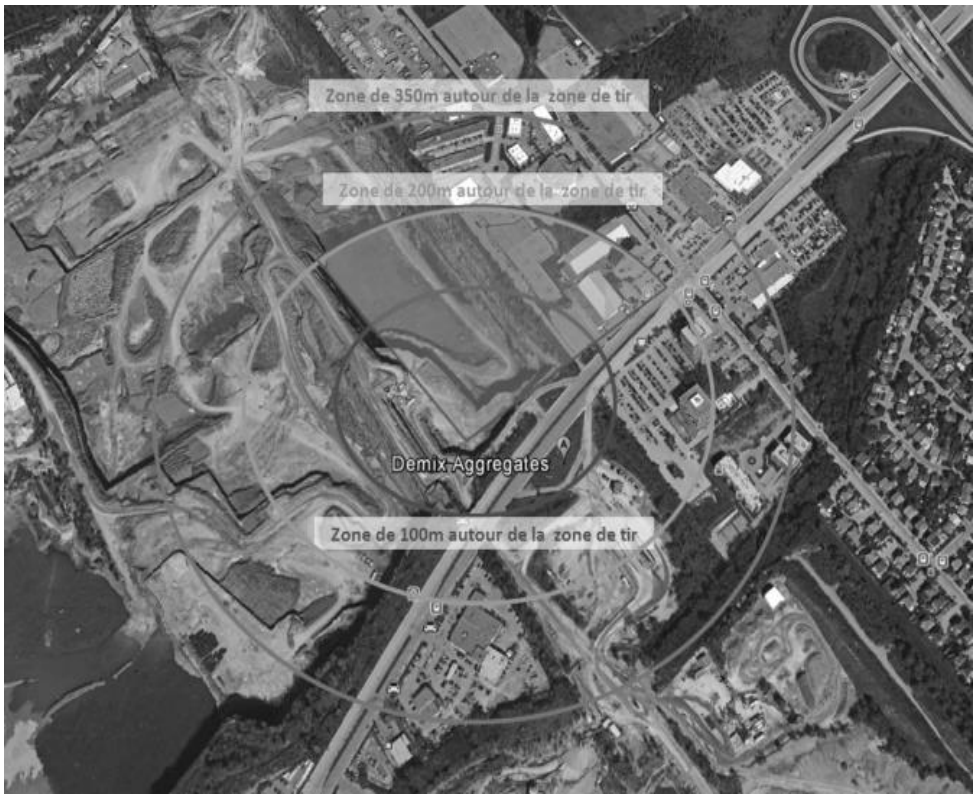

Figure 19. Zone of clearance.

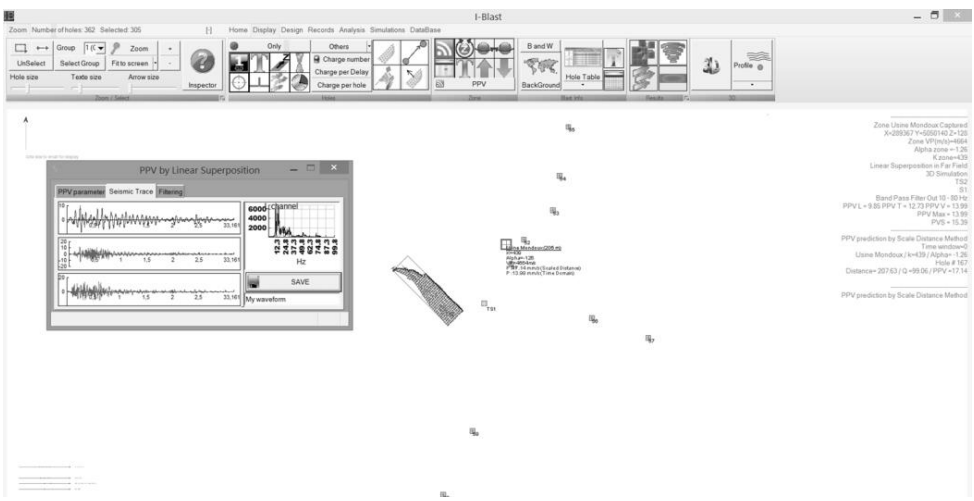

Figure 20. Vibration simulation.

360 holes were loaded with an average of 3 decks. An average of 12 people loaded the shot holes during 5 days. 73,000 kg (160,600 pounds) of explosives were used for this purpose. 2,100 electronic detonators were programmed. The duration of the blast was 2.422 seconds.

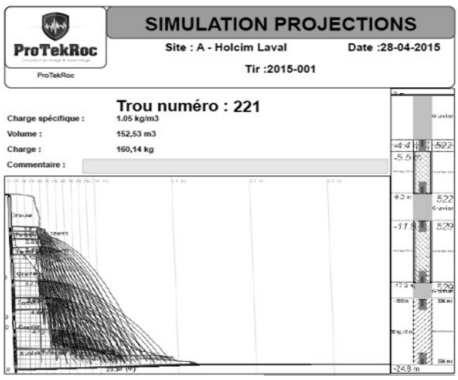

Figure 21. Projection simulation.

Figure 22. First row - loading operation.

Figure 23. Crew during loading.

Figure 24. Electronic detonators setup.

Figure 25. Electronic logger boxes used.

Figure 26. Seismograph programming.

Figure 27. Blast in motion.

17 DAY OF BLASTING

12 electronic loggers were necessary to initiate the blast. 6 seismographs were used to monitor the vibration and the air overpressure. 4 high speed cameras were placed at different angles. 22 people were present to control access during the blasting procedures. The police and the firefighters of Laval were present during the blast to assist us with security measures.

18 CONCLUSION

The technology and the tools available today enable us to perform such work safely. Following the data collection and a 3D modelling, it was possible to realise several analyses and simulations that have allowed us to realise the blast safely in compliance with the criteria set by the owner and the standards for this type of project. The monitored vibrations were about 12.5 mm/s as planned (0.5 in/s); the air overpressure was below 128 db. We observed an excellent control over the projection. The blast has presented a very good fragmentation. We obtained excellent results as for the final wall. The spread of the blast was lightly under expectation; this parameter will be improved with the next blast. In all, the Holcim direction was pleased with the result, the main goals were achieved with respect to the environment and the standards set. The second blast is planned to be done by the end of 2015.

Figure 28. Before the blast.

Figure 29. After the blast.

Figure 30. Group picture.

Stockholm Conference Proceedings 2017, R. Holmberg et al

Rectangular and circular explosive charges - detonation study using high-speed video.

M. Araos & I. Onederra
School of Mechanical and Mining engineering, The University of Queensland & Mining

ABSTRACT: Explosives are characteristically circular in shape (cylindrical charge). Square and rectangular shapes have been less studied and therefore the behaviour of the explosives in that type of packaging is less known. Usually that thickness (for slab explosives) is smaller than the critical diameter (circular cross section), which means that the shape of detonating explosives is important. In this work, the detonation process of both circular and rectangular charges was studied. A high-speed camera set at 100,000 frames per second was used to measure the performance of these different charges including velocity of detonation (VOD) and direct observations of the detonation reaction. It was originally expected that there would be a difference between the VOD of slabs and cylindrical shaped charges, as has been reported in previous work. However, no difference in VOD was measured; and further analysis of the high-speed video footage did not provide any conclusive evidence of difference, either in the length of the reaction zone or the angle at which the gases expand. Some hypotheses are suggested to explain the observed similarities in the charge configurations tested.

1 INTRODUCTION

One of the many ways to characterise an explosive (either ideal or non-ideal) is by measuring the velocity of detonation (VOD), as the process is simple and affordable. Other ways that can be used include detonation pressure, gap tests, underwater detonations, etc. Most of these types of tests are conducted when the explosive is packed in a circular shape (cylinder) as this is the shape of typical blastholes. However, there are other types of shapes, like conical in shaped charges for military or oil and gas use, which have shown the advantage of changing the shape of the packing for the explosives to perform a different task. Other explosive shapes like rectangular (to form a slab) are used for metal welding.

There is evidence that, for military explosives (Ramsay 1985) or ammonium nitrate based explosives (Petel *et al*. 2007, Silvestrov *et.al.* 2008), the thickness to the critical diameter showed that the critical thickness is approximately half of the critical diameter. Jackson instead uses the term R(VOD)/T(VOD) as a comparison of the cylinder radius and slab thickness that give an identical detonation velocity in the two geometries for the same confinement conditions (Jackson 2013).

In the last couple of years, a new non-ideal explosive has been developed in Australia and work has been done to characterise its performance. To prepare this new explosive mixture, hydrogen peroxide (HP) was mixed with fuel and then sensitised with voids. Details of this research have been published elsewhere (Araos & Onederra 2013, 2015). In this project, work was undertaken to characterise the detonation of this explosive (through VOD measurements) when packed as a slab and compare the results with cylindrical charges.

The test design varied the thickness (T) and the width (W) of the explosive slab. Both T and W increased from 25 to 100 mm (4 times the initial thickness or width of the explosive). This allowed us to detonate square and rectangular slabs. Explosive circular pipes (cylinders) with a diameter (D) of the same dimension as T or W were also detonated to compare the VOD. The detonation process of these charges was recorded using an ultra-high speed camera at 100,000 frames per second. This allowed us to measure the VOD and observe the reaction zone of the explosive and expansion of gases.

2 EXPERIMENTAL PARAMETERS

The explosive used in these tests consisted of a mixture of HP and fuel, which was mixed and sensitised at the blasting site, at a temperature of 25 – 30ºC. The formula for the explosive is shown in Table 1. This type of formula has been previously characterised and reported (Araos & Onederra 2013, 2015).

Table 1. Composition of HP/fuel-based explosive.

	Value
HP 100% (%)	41.5
Water (%)	41.5
Fuel (%)	17.0
OB	-0.24
Density (g/ml)	1.20

The sensitisation was achieved by injecting N_2 gas as the gassing agent after the oxidizer and fuel phases were mixed. A stirrer attached to a hand drill was used to disperse the N_2 bubbles throughout the mixture. The N_2 gas was sourced from a gas specialist warehouse. The final density of the explosive for all tests was 0.80 g/ml (± 0.02 g/ml). The explosive samples were loaded in rectangular and circular cross section pipes. Figure 1 displays a picture of the rectangular pipe which was made of clear acrylic sheets. Clear circular pipes were sourced from a local supplier and were made from Polyethylene terephthalate. Both types of pipes had marks every 50mm along the side, which were used to calculate the VOD when analysing the high-speed video of the detonation. The length of the pipes was 600 mm.

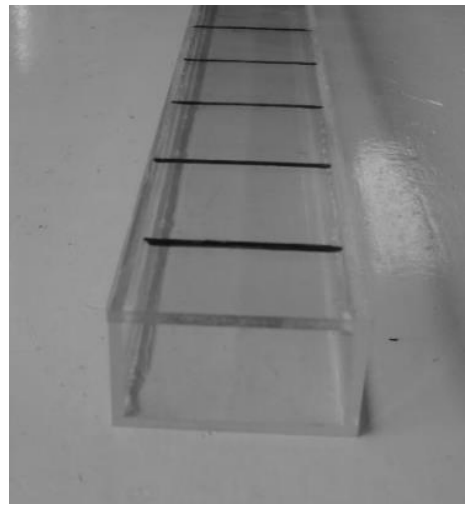

Figure 1. Picture of rectangular pipe (Slab), showing marks at 50 mm intervals.

The dimensions of both charges used in this study are given in Table 2. T and W dimensions were 25 mm, 50 mm and 100 mm, which means that the dimension varied from 1T, to 2T to 4T.

Table 2. Dimension of the pipes.

Circular pipes	Rectangular pipes	
Diameter (mm)	Thickness (mm)	Width (mm)
25	25	25
50	25	50
100	25	100
	50	50
	50	100
	100	100

To measure the velocity of detonation (VOD), the explosive charges were suspended to avoid any confinement and ground damage. Explosives were initiated with detonators and 25-grams booster. In order to see the detonation process of the explosives, the video footage of the detonation was taken using a Photron SA-X2 Colour High-Speed Camera. The footage of the detonation was captured at a speed of 100,000 frames per second. For a product detonating at 2500 m/s, the camera, at 100,000 frames per second, captures a frame every 25 mm along the detonating pipe. This means that for a pipe 600mm in length, the camera captures around 10-20 usable frames to calculate the VOD at steady state. It was noted that the first couple of frames during the detonation show a mixture of both the detonation of the booster and initiation of the explosive charges, which are not useful to measure VOD. Figure 2 below displays the location of the camera as well as the setup of the charge. As a redundancy to measure the VOD, a standard resistive wire technique (*i.e.* Microtrap MREL) was used. The measurement cable was attached to the exterior of the pipes.

Figure 2a. Test set up.

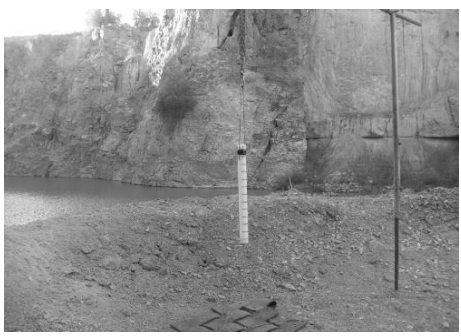

Figure 2b. Test set up.

3 EXPERIMENTAL RESULTS

HP/Fuel based mixtures, at density 0.80 g/ml, were tested in circular and square / rectangular pipes. The VOD of the explosive charges when using these shapes are displayed in Table 3. The first part of the table displays the VOD measured by using the frames of the high-speed video and the second part of the table the VOD using the Microtrap instrument. The greyed cells indicate the VOD for square pipes. The last column shows the VOD for circular pipes.

Table 3.

	VOD (m/s) – High Speed Camera			
	Width shaped pipe (mm)			Circular pipe
Thickness (mm)	25	50	100	
25	3079	3339	3332	3148
50	--	3587	3810	3640
100	--	--	3934	3995
	VOD (m/s) – Microtrap instrument			
25	3214	3421	3456	3233
50	--	3774	3824	3721
100	--	--	4167	4200

3.1 VOD for square pipes compared with circular pipes

The plot in Figure 3 displays the VOD for square pipes where the side of the pipes (T or W) has the same dimensions as the diameter (D) of the pipe. The plot shows that in fact there is no VOD difference between both types of shapes. It is observed that the VOD reaches a limit at around 4300 – 4400 m/s.

3.2 VOD change when increasing the width of the pipes

The VOD of pipes whose W increased (and keeping constant T) was studied. Figure 4 displays the results. An additional axis was added to the plot (top axis) that displays the dimensions in

'Thickness' scale (1xT…4xT). The width of the pipes varied, from 25 mm (which is a square pipe 25 mm thickness by 25 mm width) to 100 mm (25 mm thick by 100 mm width, which is equivalent to 4 x thickness). It is observed that the VOD tends to move towards a limit of approximately 3400 – 3500 m/s. After the width of the pipe equals 2 times the thickness, the VOD does not increase as much. However, this may be valid for thickness and width dimensions below 100mm. It would be difficult to see this behaviour in a rectangular pipe, for example, 150 mm x 450 mm (2 times the thickness). When the dimensions are larger than 100 mm, the explosive is closer to the ideal detonation and therefore we assume that for pipes 150 mm x 300 mm or 150 mm x 600 mm, the VOD still be the same.

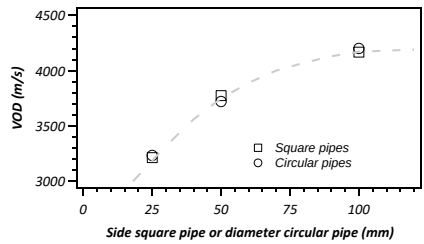

Figure 3. VOD comparison between square and circular pipes.

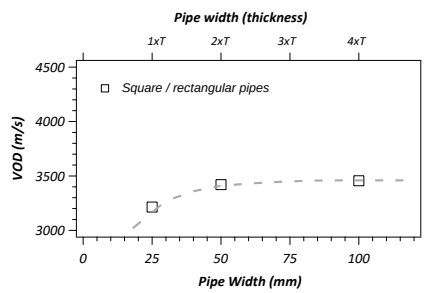

Figure 4. VOD of pipes when the width of pipe varies from 1 x thickness to 4 x thickness.

3.3 High speed images of detonations

Figure 5 displays images of the detonation process. Images of the slabs 25 x 25 mm, 25 x 50 mm and 25 x 100 mm are shown. Unfortunately, due to the speed of the footage (100,000 frames per second), the resolution is not quite good. However, by close observation of the detonation front, we can see some curvature, especially in the square pipe 100mm x 100mm. It is also worth noting the length of the potential reaction zone which appears to be more than 50mm in each of them. The colour of the gases is also an interesting feature, but this maybe an effect of the lens diaphragm aperture, rather than the actual colours for the gases themselves.

4 DISCUSSIONS

4.1 Comparison of square and circular cross section

It was shown in Figure 3 that the VOD of the explosives did not display any difference, regardless of the shape of the explosive, either square or circular. In order to compare the influence of the cross section on the VOD, Equation 1 below will be used:

$$\text{Influence of cross section} = \frac{\text{VOD (square cross section pipe)}}{\text{VOD (circular cross section pipe)}} \quad (1)$$

Table 4 shows in the right-hand side column, the ratio between the two VOD (square shape and circular shape). It can be seen that the value of the ratio is close to 1 in the entire range, regardless of the method to measure the VOD (high-speed camera or resistive wire).

Table 4. Comparison of VOD for square and circular cross section pipes.

	Size (mm)	VOD (m/s) Square pipe	VOD (m/s) Circular pipes	$VOD_{square}/VOD_{circular}$
Microtrap	25	3214	3233	0.99
	50	3774	3721	1.01
	100	4167	4200	0.99
High speed camera	25	3079	3148	0.98
	50	3587	3640	0.99
	100	3934	3995	0.98

Previous work (Petel *et al.* 2007, Silvestrov *et al.* 2008) shows that the VODsquare/VOD

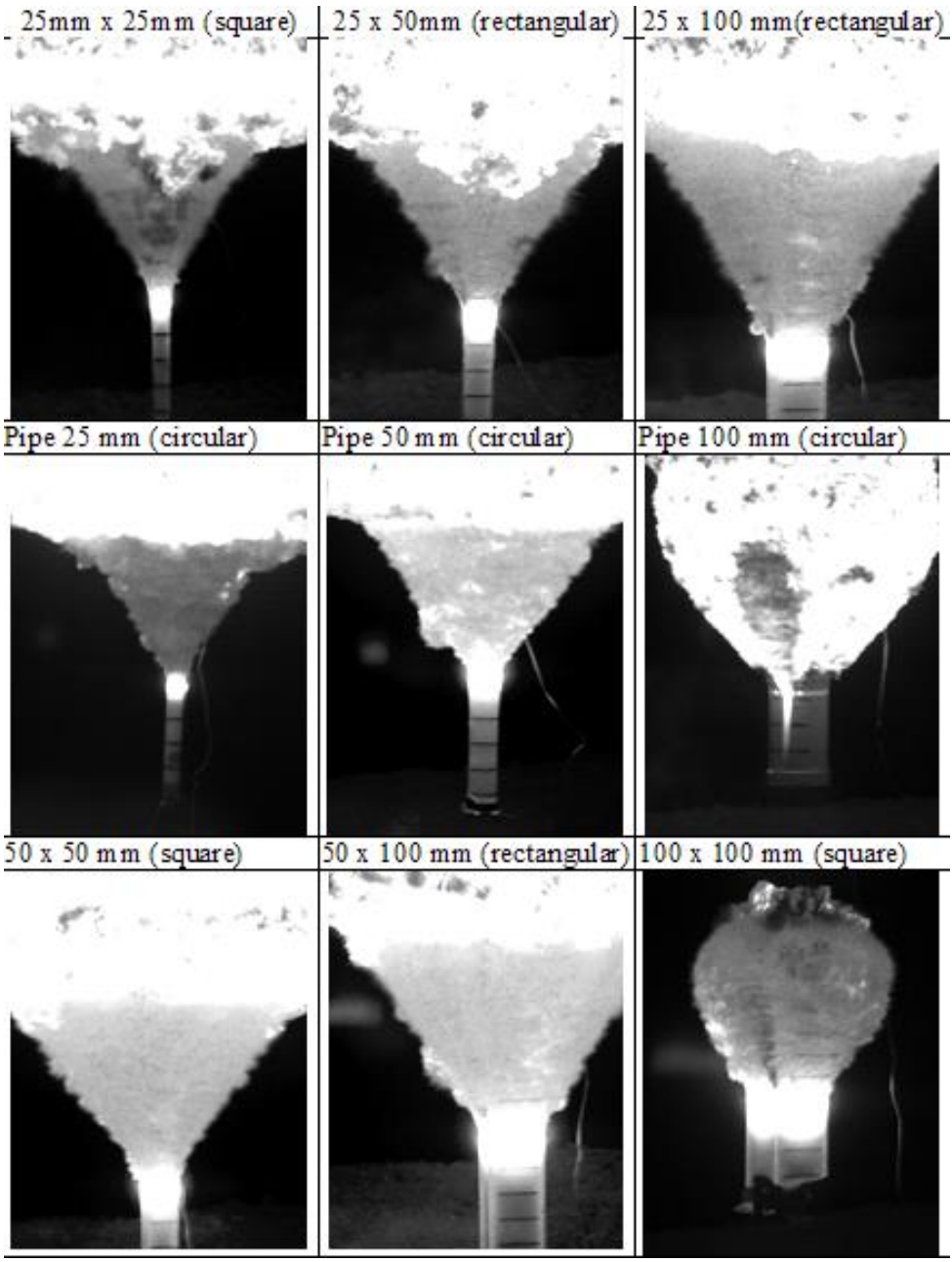

Figure 5. Frames of the detonation process for square, rectangular and circular cross section pipes.

circular, when T = D (circular pipe), is at least 1.5. If we compare the cross section of the square with circular pipes, it is seen that the square pipes have 27% more surface:

The larger surface for the square pipe does not influence VOD. It is hypothesised that T/D ~ 1 in this work has been due to the type of tests. Most of the work conducted in the past, either with high

explosives or non-ideal explosives, has been related to the comparison of slab and circular pipes at the critical T value for slabs and critical D value for circular pipes. In our case our tests were well above those critical dimensions and hence any losses of heat during the detonation process cannot influence the VOD. However, more testing should be conducted to reach a definitive conclusion.

$$Ratio\ surfaces = \frac{Surface\ squre\ pipe}{surface\ circular\ pipe} = \frac{T \times T}{radius^2 \times \pi} =$$

(cont.)
$$\frac{T^2}{\left(\frac{T}{2}\right)^2 \times 3.14} = \frac{4 \times T^2}{T^2 \times 3.1416} = \frac{4}{3.14} = 1.27 \quad (2)$$

4.2 Change of VOD with width

No previous work has been found on this type of experiment that allows us to compare or have a starting point. Our results showed that the VOD tend towards a maximum for pipes whose width is > 2x thickness. When plotting 1/Diameter of pipe Vs VOD for that diameter, it is possible to extrapolate to the VOD for an infinite diameter. The results of this work are showing that for rectangular cross section pipes, the infinite VOD can be calculated when the width is around 3 – 6x the thickness.

We can see that, despite the limited number of shots, the VOD tends to a limit for both types of shapes. This is expected as at infinite diameter the type of shape of the explosive should not have any influence.

4.3 High speed video analysis

The high-speed footage allowed us to observe the reaction zone. Images shown in Figure 5 depict a bright area preceding the expanding gases. This bright area is relatively well defined, and it is assumed that the reaction is occurring in that area and hence the bright light released. It is difficult to assume that the bright zone is caused by the detonation front reaction's light filtering forward. If that were the case, the brightness will decay smoothly, not having a boundary like the ones seen in the images.

The definition of the pictures from the high-speed footage does not allow for a clear measurement of the length to make a comparison between the length of the reaction zone for the slab and for circular charges. We would be able to say that the there is no significant difference. The reaction zone is at least 50 – 70x larger than the reaction zone of high explosives. The length of the reaction zone observed in this work appears to contradict the general theory of detonation, where reaction zone lengths are expected to be a few mm in length (Campbell 1976, Silvestrov 2008). Therefore, further studies are needed to determine if the assumptions in this paper regarding the reaction zone length can be confirmed or not.

As far as the expanding gases are concerned, no difference can be observed for any of the shapes. However this may be due to the position of the camera. If the camera was in a different angle, gases could have shown a different expansion, due to the corners of the rectangular cross section of the pipes.

5 CONCLUSION AND FUTURE WORK

This experiment measured the VOD of explosives packed in different shapes (circular, square and rectangular). The results of the ratio VOD-square/VODcircular obtained in this work are different to previous work, where the VOD of rectangular cross section pipes are higher than a cylindrical pipe.

Experimental work has shown that for square pipes where the side of the pipes (T or W) has the same dimensions as the diameter (D) of the pipe, there is no VOD difference between both types of shapes. It was also observed that the VOD reaches a limit at around 4300 – 4400 m/s.

The larger surface for the square pipe does not influence VOD. It is hypothesised that that T/D ~ 1 in this work has been due to the type of tests – previous work aimed to find the critical dimensions of the detonation (critical diameter or critical thickness). However, more testing should be conducted to reach a definitive conclusion.

High speed video of the detonation process for a new explosive based on HP/fuel and sensitisation has been presented. Although the initial aim for this research was to see the reaction zone, the analysis of the videos found some other interesting characteristics that may help understand the detonation process for non-ideal explosives. Additionally, work needs to be done on the video resolution. At this moment, the resolution is acceptable, but it needs to be improved, so the details of the reaction zone can be seen with more definition.

Further work is planned to achieve that understanding with ammonium nitrate-based explosives included in future studies.

6 ACKNOWLEDGEMENTS

The assistance of Nathan Newton and Virginia Bailey (MSc student from University of Queensland) Lee Hayter (from EXTECH) and Ridley Williams (from Slowmotion Australia), is greatly appreciated. The assistance of ACARP, by granting the funds for the HP-based explosive research, is also appreciated.

REFERENCES

Araos, M. & Onederra, I. 2013. Detonation characteristics of alternative mining explosives based on hydrogen peroxide. *7th World Conference on Explosives & Blasting*, Moscow, Russia, Sep. 13-15, 2013, pp. 182-186.

Araos, M. & Onederra, I. 2015. Development of a novel mining explosive formulation to eliminate nitrogen oxide fumes. *Mining Technology*, 124, pp. 1-23.

Campbell, A.W. & Engelke, R. 1976. The diameter effect in high-density heterogeneous explosives. *Proceedings 6th Symposium (International) on Detonation*, ACR-221, 642-652.

Jackson, S.I. & Short, M. 2015. Scaling of detonation velocity in cylinder and slab geometries for ideal, insensitive and non-ideal explosives. *Journal of Fluid Mechanics* 773, 224-266.

Petel, O.E., Mack, D., Higgins, A.J., Turcotte, R. & Chan, S.K. 2007. Minimum propagation diameter and thickness of high explosives. *Journal of Loss Prevention in the Process Industries*, Vol.20(4), 578-583.

Ramsay, J.B. 1985. Effect of confinement on failure in 95TATB/5 KEL-F. *In Proceedings of the 8th international symposium on detonation*, 372–379.

Silvestrov, V.V., Plastinin, A.V., Karakhanov, S.M. & Zykov, V.V. 2008. Critical diameter and critical thickness of an emulsion explosive. *Combustion, Explosion, and Shock Waves*, 44, 3, 354–359.

Stockholm Conference Proceedings 2017, R. Holmberg et al

Detonation performance of novel hydrogen peroxide and nitrate based hybrid explosives

I. Fullelove, M. Araos & I. Onederra
The University of Queensland, School of Mechanical and Mining Engineering, Mining3, Australia

ABSTRACT: Recent developments have indicated that explosive mixtures of hydrogen peroxide (HP) and fuel exhibit detonation performance characteristics that could potentially make them viable for use in the civil and mining industries to fragment rock. Further development of the technology has also involved the study of hybrid mixtures containing combinations of HP and nitrates in the oxidiser phase of the explosive. These oxidiser mixtures allowed a study of the influence of the nitrate's cation on the detonation performance of the explosives. Performance was characterised by both detonation modelling and a series of fully instrumented unconfined velocity of detonation (VOD) tests. Analysis showed some interesting differences in the velocity of detonation between the hybrids using Na^{+}, NH_4^{+} and Ca^{+2}. Hybrid mixtures of peroxide with sodium nitrate showed that even though there is theoretically more energy available, field results indicate that this extra energy does not translate into higher velocities of detonation for a range of densities. Additionally, variation in the charge of the cation in the nitrate (*i.e.* Na^{+}, Ca^{+2}) does not translate into a significate difference in VOD, which suggests that cation charge does not influence detonation performance. Some hypotheses are offered to explain this behaviour.

1 INTRODUCTION

Since the Texas Port disaster of 1947, there has been a steady increase in the use of ammonium nitrate based explosives (*i.e.* ANFO, emulsions, water gels, etc.), which are now the most widely used bulk commercial explosive in the mining, quarrying and civil industries. Explosive suppliers and manufacturers have established ammonium nitrate (AN) as their primary commodity, with large investments into the infrastructure required for the manufacturing, storage and use of AN. Because of this, independent research and development into alternative explosive formulations has been limited in recent decades. However, as the production of hazardous nitrogen oxide (NOx) fumes from the use of AN based explosives continues to present a serious safety risk, researchers are beginning to consider alternative explosive formulations.

With the aim of eliminating the NOx fume hazard, a novel explosive formulation was developed by Araos and Onederra (2013) that utilises hydrogen peroxide (HP) instead of ammonium nitrate as the primary oxidising agent. The detonation performance of this new HP/fuel explosive product has been thoroughly studied by Araos and Onederra (2013, 2015), and Onederra

and Araos (2017). Results of unconfined velocity of detonation (VOD) tests conducted by these investigators have shown that HP/fuel explosive mixtures exhibit non-ideal detonation performance characteristics similar to current AN based commercial explosives.

Research conducted by Araos and Onederra (2013, 2015) has created the opportunity for the development of a new group of potential commercial explosives that do not require AN as their primary oxidising agent. However, it is well known that HP is an excellent oxidiser which is highly reactive with many classes of chemicals but is also known for being particularly challenging to handle and store (Mackenzie 1990). This would be problematic for explosives that use HP as their primary oxidising agent, as large amounts of HP are required. It was initially hypothesised that the addition of a nitrate to the oxidiser phase of HP/fuel mixtures would reduce the amount of HP required in the formulation; extended the range of product densities; improve the stability and handling characteristics of the product; and still contain less nitrogen than existing AN based commercial explosives. Therefore three novel explosive formulations were developed, each containing a hybrid mixture of hydrogen peroxide and either sodium nitrate (SN), calcium nitrate (CN) or ammonium nitrate (AN). In order to investigate the potential of these novel hybrid explosives, their detonation performance was characterised by both detonation modelling and a series of unconfined velocity of detonation tests.

2 REVIEW OF HYDROGEN PEROXIDE AND NITRATES USE IN EXPLOSIVE PRODUCTS

Ammonium nitrate forms the primary oxidising agent of nearly every currently available bulk commercial explosive product. The use and non-ideal detonation characteristics of AN based explosives have been extensively studied and published for many years (Hagan 1968, Lee *et al.* 1989, Persson *et al.* 1993). It is well known that the oxidiser composition of AN based explosives influences their detonation performance (Frost & Zang 2009). SN and CN are regularly added in small quantities to the oxidiser phases of AN based slurries and emulsions to improve their explosive characteristics or for stability and economical reasons, but are not used as the primary oxidiser in any currently available bulk commercial explosives (ISEE 2014). It has been hypothesised that because the heat of formation of SN and CN during detonation is lower than that of AN, they would exhibit poorer explosive performance (Mahadevan 2013). Lee *et al.* (1989) also suggested the slower VOD exhibited by emulsions containing combinations of AN/CN and AN/SN compared to emulsions containing only AN in the oxidiser phase were due to the slower rate of decomposition of the metallic salts. Nonetheless, there has only been limited study of the effect on the detonation performance of bulk explosive products due to the individual nitrate's cation (*i.e.* Na^+, NH_4^+ or Ca^{+2}) in the oxidiser phase. Hybrid mixtures containing HP with different nitrates has allowed a study of the influence of the nitrate's cation on the detonation performance of these particular explosives.

The first recorded detonation of HP-fuel based explosive mixtures was published by Shanley & Greenspan (1947). In 1948, Shanley & Kauffmann (1948) obtained a patent for the use of hydrogen peroxide, glycerol and water as a single-phase liquid explosive. The explosive limits are illustrated in the ternary diagram for the explosive in Figure 1. The work by Shanley & Kauffmann (1948) was significant because provided the water content was below 52%, HP/fuel mixtures were found to detonate from a standard blasting cap.

In 1962, Baker & Groves (1962) were granted a patent for a formulation that utilised explosive mixtures of high concentration HP and a range of solid fuels. One of the most important and novel breakthroughs by Baker & Groves (1962) was their discovery that the amount of HP in the explosive mixtures could be reduced by adding other oxidising agents such as sodium nitrate or ammonium nitrate. A patent granted to Bouillet *et al.* (1990) was for cartridge explosive mixtures that contained high concentrations of HP (>60% w/w), oxidising organic material and a gelling agent. These packaged explosives detonated with a VOD in the order of 6,000 m/s in unconfined PVC tubes, with densities in the range of 1.20-1.38 g/cc.

Recently, Araos & Onederra (2013, 2015) illustrated from a series of unconfined VOD tests that mixtures of a lower concentration of HP (44% w/w) and a fuel were able to detonate if adequetly sensitised. The mixtures detonated over a range of densities in small diameter tubes (*i.e.* 23 mm to 87 mm) at velocities between 2,600 m/s and 5,000 m/s, as illustrated in Figure 2 (Araos & Onederra 2013, 2015). The velocities at which the sensitised HP/fuel mixtures detonated are comparable with currently available commercial ANFO, emulsion

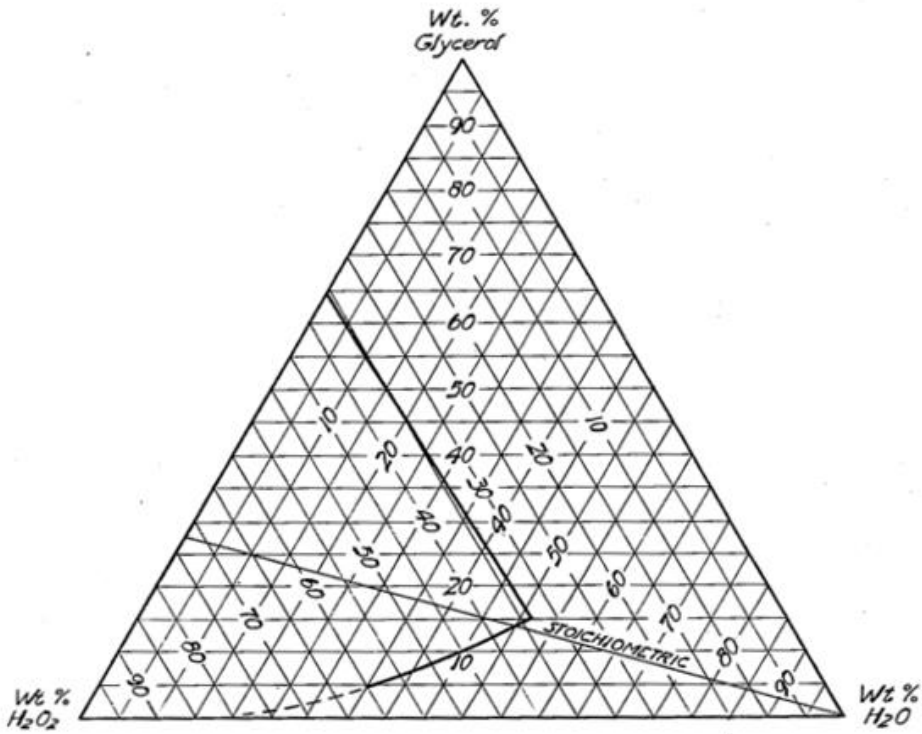

Figure 1. Range of explosive compositions for glycerol-peroxide-water mixtures (Shanley & Kauffmann 1948).

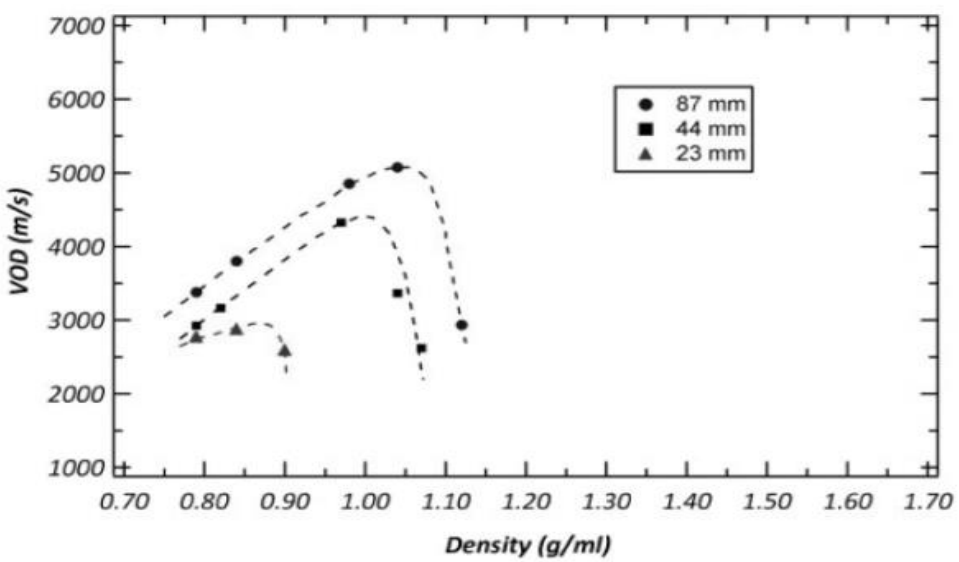

Figure 2. VOD of explosive HP/fuel mixture for different diameters and densities (Araos & Onederra, 2013).

and water gel technologies. The work by Araos & Onederra (2013, 2015) is significant because previous research by other scholars had found that only explosive mixtures with high concentrations of HP above 60% w/w were able to detonate with reasonable velocities (Heemskerk & Scholtes 1996, Schreck *et al.* 2004, Sheffield *et al.* 2010). However, the effect on detonation performance of adding nitrates to sensitised low-concentration HP/fuel explosive mixtures has not yet been studied. As nitrates and HP both have positive oxygen balances, it was hypothesised that a certain amount of HP in the HP/fuel mixture could be replaced by nitrates and detonation would still be possible.

3 FORMULATION OF NOVEL HYBRID EXPLOSIVES

Three novel hybrid explosives were developed, each with a different nitrate in the oxidiser phase. This was done in order to explore how the detonation performance of the novel hybrid product is affected by the nitrate's cation used in the oxidiser phase. The oxidiser phase of the three hybrid explosives contained water, hydrogen peroxide (HP), and either sodium nitrate (SN), calcium nitrate (CN) and ammonium nitrate (AN). These three nitrates were chosen because they are commonly available chemicals and are already used in currently available bulk commercial explosives.

The primary objective for comparing the detonation performance of the hybrid explosives was to keep the proportion of the nitrates in the oxidiser phase and oxygen balance of the explosive mixture constant across all three explosive formulations. This would ensure an unbiased comparison of the effect of different nitrates on the detonation performance. The secondary objective was to use the highest concentration of nitrate in the oxidiser phase as possible, so the difference in the detonation performance of the three hybrid explosives would be observable. However, due to the low solubility of SN, the oxidiser phase of each novel hybrid explosive was limited to 35% w/w nitrate, 24.8% w/w HP, and 40.2% w/w water. Note that these are the percentages by weight of the chemicals in the oxidiser phase, not the total explosive mixture.

The fuel phase of the three hybrid explosives was comprised of a water-soluble liquid fuel and a thickening agent used to modify the viscosity of the explosive gels. Density control and sensitisation of the explosive gels was achieved by the addition of Glass Micro Balloons (GMB) Q-Cel 5020 (from Potters Australia) to the gel. The relative proportion of the thickening agent used in the fuel phase of each hybrid product was dependent on the GMB. If the gel wasn't viscous enough, then the GMB would separate out from the gel and float, but if the gel was too viscous, then the GMB would not sufficiently mix through the gel. The proportion of thickening agent that was found to produce a suitable viscosity for each hybrid explosive ranged between 0.6% w/w and 1.0% w/w of the total formulation. The unsensitised gel densities of the three novel explosive formulations are presented in Table 1. GMB was added in different amounts to produce sensitised hybrid explosive products with densities ranging from 0.50 g/cc to 1.35 g/cc.

The oxygen balance (OB) of an explosive is a vital characteristic of its formulation, as the detonation performance of the product is strongly dependent on how much oxygen is available in the

Table 1. Relative proportion of chemicals used in hybrid explosive products.

Chemical	SN/HP/Fuel (% w/w)	CN/HP/Fuel (% w/w)	AN/HP/Fuel (% w/w)
SN	28.28		
CN		28.18	
AN			30.21
HP	20.05	19.98	21.42
Water	32.47	32.34	34.67
Fuel	19.20	19.50	13.70
Oxidiser : Fuel	80.8 : 19.2	80.5 : 19.5	86.3 : 13.7
OB %	-0.55	-0.51	-0.45
Gel density (g/cc)	1.34	1.35	1.25

explosive for consumption during detonation (Akhaven 2004). The closer an explosive is to being oxygen balanced, the more energy will be released during detonation (Liu 2015). However explosive manufacturers typically maintain a slightly negative OB for their AN based explosives as this reduces the likelihood of a NOx fume event (ISEE 2014). For this reason, the OB of the three hybrid explosives was maintained between -0.45% and -0.55% by using an appropriate oxidiser to fuel ratio. The formulation of the hybrid explosive products are summarised in Table 1. The weight percentage of nitrate, HP and water were similar for all three products, with HP concentrations of approximately 20% w/w.

4 IDEAL DETONATION MODELLING

Before conducting fully instrumented field testing of the formulated novel hybrid explosives, detonation code modelling was completed to estimate their ideal detonation performance. A detonation code developed as part of a major research project at the University of Queensland was utilised in this research project. The code utilises both fundamental thermo-chemistry and hybrodynamic principles as the basis for its analysis. Modelling of the detonation properties of the hybrid explosives was valuable because it provided an estimation of the maximum attainable performance of each of the explosives, irrespective of their diameter or confinement. The detonation properties that were modelled for each of the novel hybrid explosives included: ideal VOD, available energy, detonation pressure, and detonation temperature. The available energy was estimated by the code as the energy released by the explosives before the pressure of the gasses fall below 100 MPa due to expansion.

The ideal VOD of the hybrid explosive products was modelled for a range of densities from 0.58 g/cc to 1.35 g/cc, as illustrated in Figure 3. As the density of the hybrid explosives increased so did their VOD, which is a standard characteristic of all explosives. The AN based hybrid product exhibited the highest ideal velocities of detonation of 3800 m/s to 6800 m/s. The SN and CN based hybrids had similar ideal velocities of detonation ranging from 3500 m/s to 6500 m/s depending on the explosive density. This was an interesting result, as SN and CN have different chemical properties but modelling suggested their hybrid explosive mixtures had comparable velocities of detonation.

The SN based explosive had the greatest available energy between 2.2 MJ/kg and 4.6 MJ/kg, which was approximately 0.5 MJ/kg greater than both the AN and CN based products, as illustrated in Figure 4. Even though the hybrid mixtures containing SN and HP theoretically have more available energy, ideal detonation modelling illustrated that more energy does not translate into higher velocities of detonation for a range of densities. Further, the modelled ideal VOD and available energy of the three hybrid products suggested that the variation of the cation charge of the nitrate (*i.e.* Na^{+}, Ca^{+2}, NH_4^{+}) does not result in a significant difference in detonation performance.

The modelled ideal detonation pressure and temperature for the novel explosives are illustrated in Figure 5 and Figure 6 respectively. All three hybrid explosives had similar modelled detonation pressures, with the detonation pressure of the AN based hybrid explosive approximately 0.5 GPa greater than both the SN and CN based products. The detonation temperatures for each of the hybrid explosives remained fairly constant over the range of modelled explosive densities, with the SN hybrid explosive exhibiting the highest detonation temperature of approximately 3800°C.

Ideal detonation modelling of the three novel hybrid explosive products offered some interesting insights into their potential performance. A different hybrid product exhibited the greatest performance for each modelled detonation property (*i.e.* VOD, energy, detonation pressure and temperature). The AN based product displayed the highest ideal VOD and detonation pressure, whereas the SN based product was predicted to detonate with the greatest temperature and available energy. Thus, modelling predicted no clear correlation between the choice of nitrate in the formulation and the resulting detonation performance.

5 UNCONFINED DETONATION TESTS

In order to fully characterise the detonation performance of the novel hybrid explosive mixtures, a total of 30 fully instrumented unconfined VOD tests were conducted at a blasting range. The only parameter altered during the detonation tests was the density of the charges. All other variables which could influence the detonation performance of the explosive remained constant. These variables included: confinement, charge dimensions, type of sensitisation (*i.e.* GMB) and initiation energy. Charges were loaded

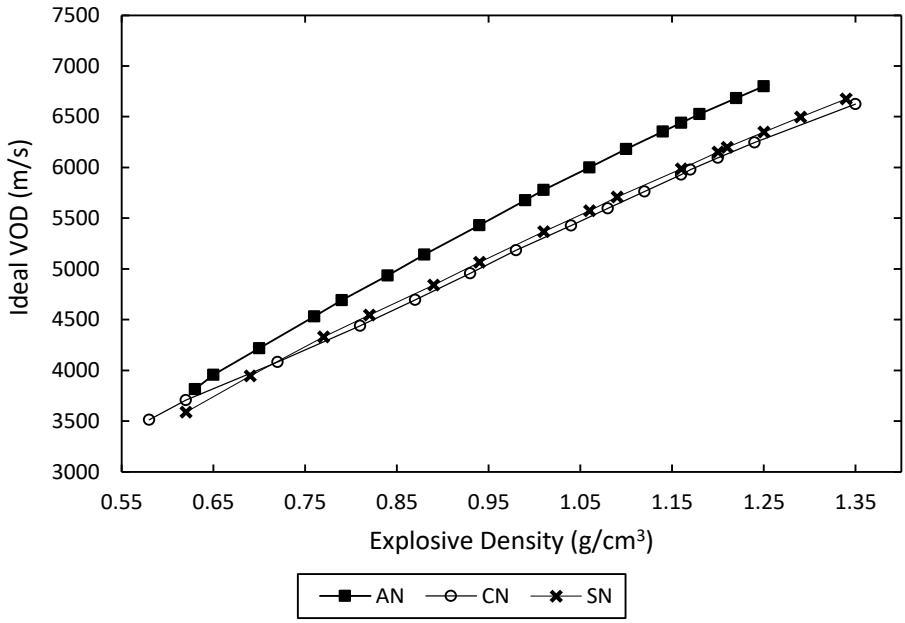

Figure 3. Modelled ideal VOD of hybrid explosive products.

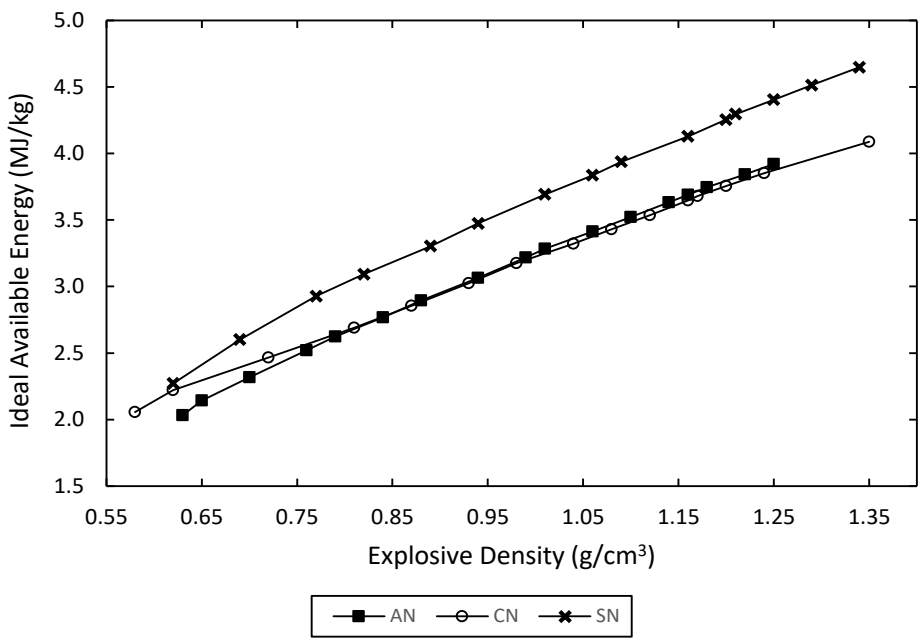

Figure 4. Modelled available energy and RWS of hybrid explosive products.

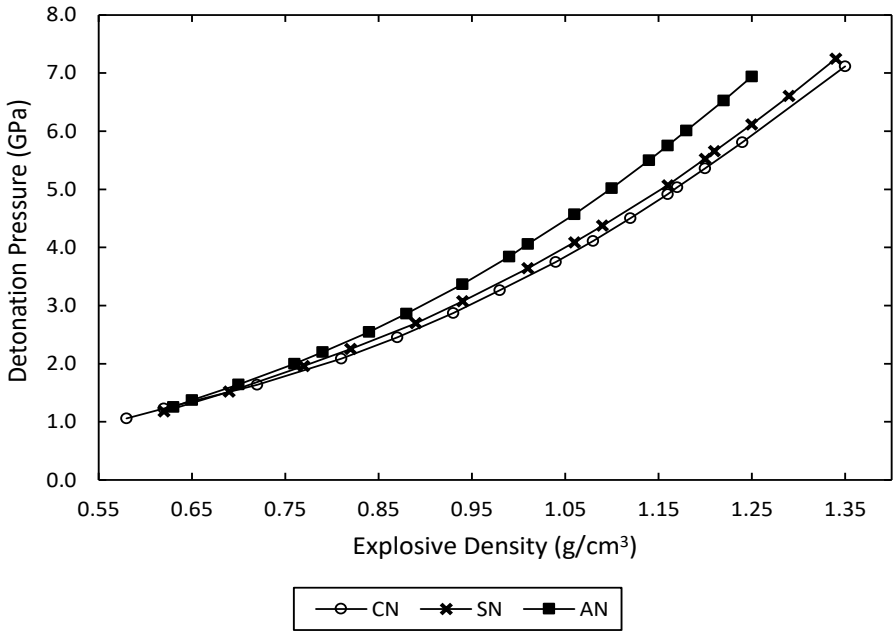

Figure 5. Modelled ideal detonation pressure of hybrid explosive products.

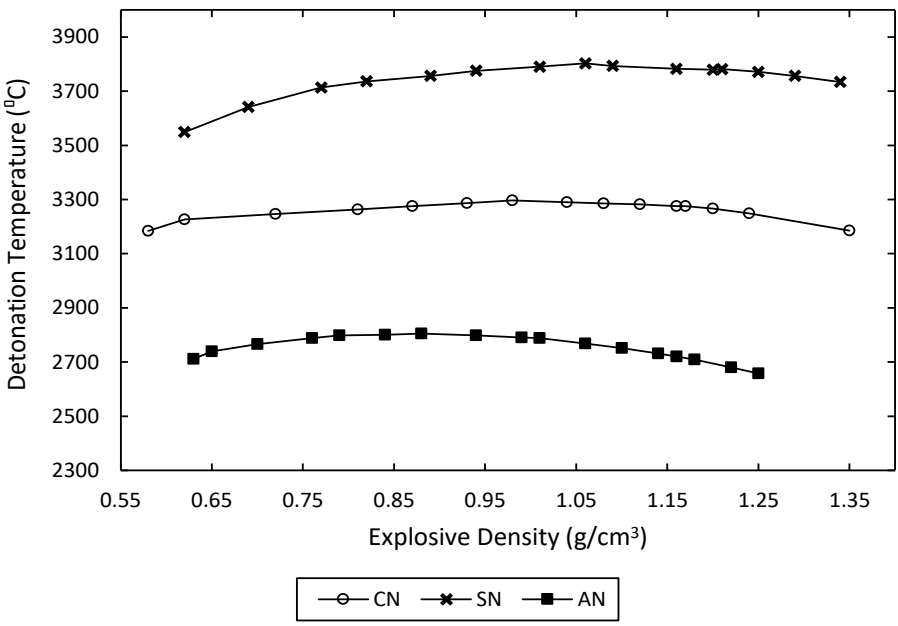

Figure 6. Modelled ideal detonation temperature of hybrid explosive products.

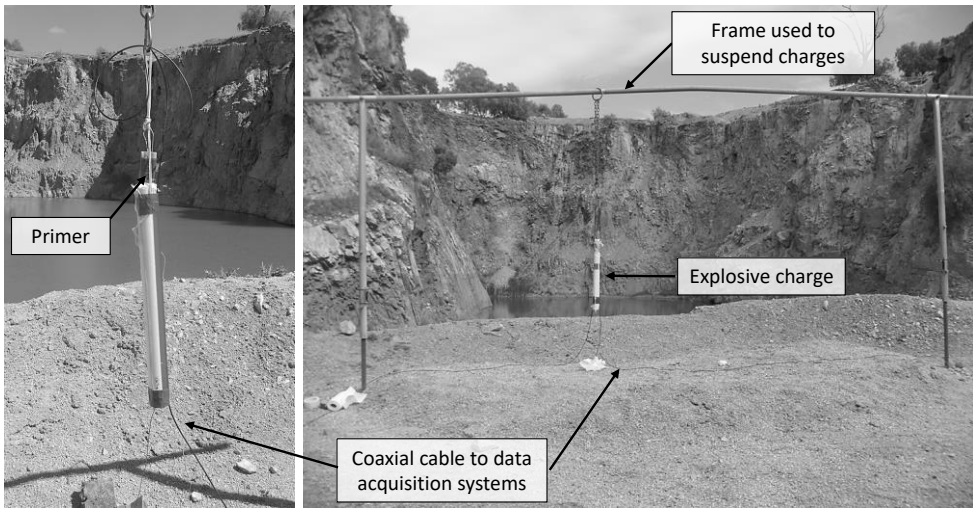

Figure 7. Setup of typical unconfined VOD test.

into tubes which were 51 mm in diameter, 600 mm long and were constructed of thin plastic with a wall thickness of 1 mm. The VOD of the explosive charges was continuously measured using both a ShotTrack VOD monitor (ShotTrack 2015) and MREL Microtrap data acquisition system (MREL 2017). Using two data acquisition systems provided a necessary redundancy and ensured that any measurement bias was minimised. The explosive charges were suspended from a metal frame, and the coaxial cables used by the VOD data acquisition systems were taped to the outside of the charge. A primer consisting of two 25 g Pentolite boosters was then used to initiate the explosive mixtures. The typical setup of an unconfined detonation test is presented in Figure 7.

Typical VOD traces recorded by the Microtrap and ShotTrack VOD data acquisition systems are shown in Figure 8. Even for explosive charge lengths of only 600 mm, a stable VOD was able to be measured for all the charges which successfully detonated. For a 51 mm diameter charge, it was found the AN based hybrid explosive produced the highest VODs over the range of charge densities tested, as illustrated in Figure 9. The AN based product detonated with velocities between 3231 m/s and 5158 m/s for densities in the range of 0.65 g/cc to 1.16 g/cc. The CN based hybrid product detonated with velocities between 2280 m/s and 4604 m/s for densities in the range of 0.51 g/cc to 1.28 g/cc; and, the SN based hybrid product

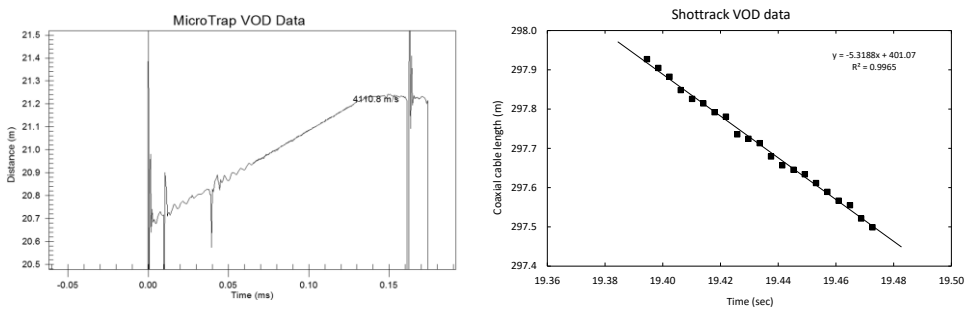

Figure 8. Microtrap and ShotTrack VOD trace for AN based hybrid explosive at 0.96 g/cc.

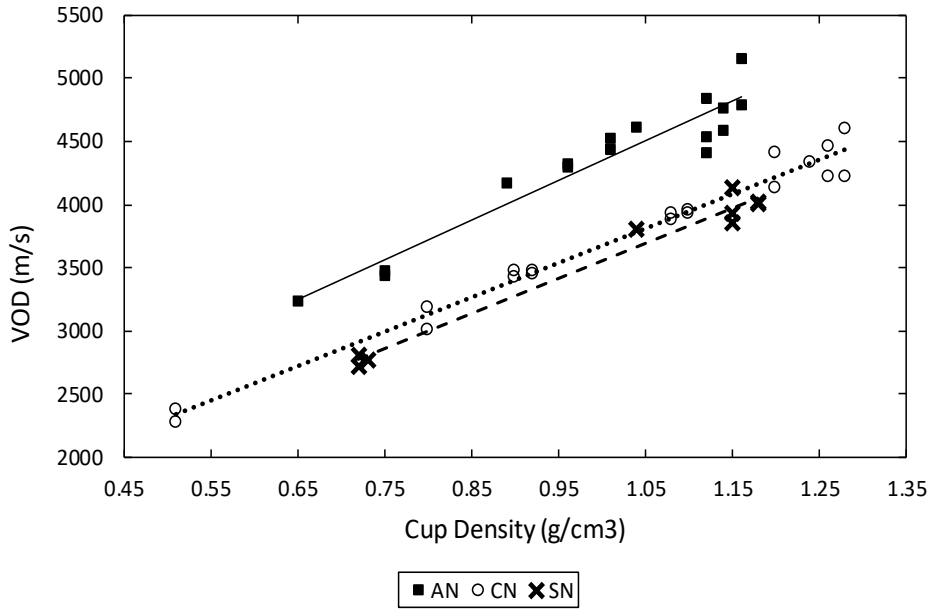

Figure 9. Unconfined VOD vs density for novel hybrid explosives.

detonated with velocities between 2720 m/s and 4133 m/s for a range of densities between 0.72 g/cc and 1.18 g/cc. The unconfined VOD test results followed a similar trend to the modelled ideal VOD results, in that hybrid explosives containing ammonium cation in their oxidiser phase exhibited higher detonation velocities than for the hybrid products containing sodium and calcium nitrate. Field testing of the hybrid mixtures of peroxide with sodium nitrate also confirmed that even though there is theoretically more available energy, this does not necessarily translate into higher velocities of detonation.

It can be inferred that the three hybrid products exhibited non-ideal detonation behaviour because their velocities of detonation were considerably lower than predicted values from ideal detonation modelling. This observed non-ideal detonation behaviour is in agreement with the findings published by Araos & Onederra (2015). For a density of 0.97 g/cc in a 44 mm tube, Araos & Onederra (2015) found that explosive HP/fuel mixtures detonated with a VOD of approximately 4300 m/s. However, at densities above 0.97 g/cc, the velocities of detonation of the HP/fuel mixtures reduced significantly to less than 3000 m/s in 44 mm tubes (Araos & Onederra 2015). All three novel hybrid explosives presented in this paper detonated at densities above 1.15 g/cc with velocities in excess of 4100 m/s. Thus the addition of nitrates to the oxidiser phases of explosive HP/fuel mixtures did not considerably increase their maximum attainable VOD, but was found to increase their VOD at higher densities.

As mentioned previously, Araos & Onederra (2015) found for HP/fuel explosive mixtures that at a certain density there tended to be a peak VOD, with higher density mixtures resulting in a lower VOD. This performance has been extensively observed and published for other sensitised bulk commercial explosives which exhibit non-ideal detonation behaviour (Price 1966, Hattori *et al.* 1982, Lee & Persson 1990). It is believed this characterstic of non-ideal detonation was not observed for the novel hybrid explosives because the difference in their peak-VOD density and critical density may have been too small.

Nonetheless, the detonation of the novel hybrid explosives at higher densities was strongly dependent on the level of sensitisation, allowing a comparison of their critical densities for a 51 mm charge diameter. The highest density at which the SN product was tested was 1.18 g/cc. However, the maximum density at which the SN product

would detonate was not able to be determined in this testing program, as all densities that were tested successfully detonated. Considering that the density of the unsensitised gel was approximately 1.34 g/cc, it can be inferred that the critical density of the SN product is between 1.18 g/cc and 1.34 g/cc for a 51mm charge. The AN based hybrid explosive detonated in a 51 mm tube at a density of 1.16 g/cc but failed to initiate at a density of 1.19 g/cc. Similarly, the CN based hybrid product detonated at a density of 1.28 g/cc in a 51 mm tube but failed to detonate at 1.30 g/cc. From these results, the CN based hybrid product appears to have the greatest critical density, followed by the SN based hybrid product, with the novel AN product having the lowest critical density. This result was interesting because the novel AN hybrid explosive actually exibited the highest VOD for the range of densities tested.

6 DISCUSSION OF THE DETONATION PROPERTIES OF THE NOVEL HYBRID EXPLOSIVES

The detonation performance of hybrid explosive mixtures containing HP and nitrates in the oxidiser phase illustrated two phenomena which have not been explained in the literature:

- more avialable explosive energy does not necessarily translate into higher velocities of detonation for a range of densities,
- the variation of the cation charge in the nitrate (*i.e.* Na^{+}, Ca^{+2}) does not translate into a significant difference in VOD

Some hypotheses are presented to explain these observed phenomena. In order for a detonation front to progress through an explosive material, there must be ignition of the reactants due to the creation of hot spots in the explosive (Bowden & Yoffe 1952, Zinn 1962). These hot spots are typically created by the compression of voids (*i.e.* GMB) in the explosive due to the shock front of the detonation, increasing their temperature until they initiate the surrounding reactants (Braithwaite 2013). The energy enparted by hot spots to the explosive reactants must be great enough to overcome their activation energies and continue the detonation reaction. It is hypothesised that even though the SN hybrid mixture theoretically had more available energy during detonation than the AN hybrid product, the activation energy of the reactants required to progress the detonation was higher for the SN hybrid mixture than the AN hybrid product. This conjecture will have to be tested in future work by assessing the activation energies of the reactants in the novel hybrid explosives. However, if the activation energy of the reactants in the SN hybrid are higher, then the rate of the detonation reaction through the product would be slower than that of the novel AN product, which was what was observed during the unconfined detonation testing. Therefore it is proposed that the velocity of detonation of non-ideal explosives is not related to the total amount of energy released during detonation, but is in fact a function of the rate at which explosive energy is released (*i.e.* the power of the explosive), which in turn is a dependent on the activation energies of the explosive reactants.

Another hypothesis is that the modelled available energy for the ideal detonation of the novel explosives is not representative of their true available energy during detonation. Ideal detonation modelling is often used to estimate the total energy released during detonation from the heat of formation of the detonation products and reactants, assuming the reaction goes to completion as the detonation front passes (Braithwaite 2013). However, commercial explosives exhibit non-ideal detonation behaviour, for which the energy released during detonation is not only dependent on the explosive formulation, but also on the detonation parameters, such as pressure, temperature, confinement and charge diameter (Mohanty 2013). Therefore, the available energies estimated by the ideal detonation code would not be a fair estimate of the energy released during the detonation of the novel products studied in this research. This may explain why higher velocities of detonation were not observed for the novel explosive products which theoretically contained more available energy.

7 CONCLUSIONS AND FUTURE WORK

Previous work has illustrated that sensitised mixtures of low-concentration hydrogen peroxide with a fuel exhibited detonation properties comparable to currently available commercial explosives. However, there have been no investigations conducted on the detonation performance of hybrid explosive mixtures containing combinations of HP and nitrates in the oxidiser phase of the explosive. Therefore three novel explosive formulations were developed, each containing a hybrid mixture of hydrogen peroxide and either sodium nitrate, calcium nitrate

or ammonium nitrate. These hybrid explosive mixtures allowed the study of the effect on explosive performance from using different cations with the nitrate in the oxidiser phase.

Modelling and a series of unconfined velocity of detonation tests were used to characterise the detonation performance of the novel mixtures. Analysis of the test results illustrated the following:

- the addition of nitrates to the oxidiser phases of explosive HP/fuel mixtures did not considerably increase their maximum attainable VOD, but was found to increase their VOD at densities above 1.00 g/cc
- for the range of densities tested, the AN based hybrid product detonated with the highest unconfined velocities of detonation, reaching over 5100 m/s at a density of 1.16 g/cc
- the SN hybrid product detonated at velocities similar to those exhibited by the CN hybrid explosive, suggesting that the variation of the cation charge of the nitrate does not result in a significant difference in detonation performance
- even though the hybrid mixtures containing SN and HP theoretically had more available energy, ideal detonation modelling and field testing illustrated that more energy does not translate into higher velocities of detonation for a range of densities

Hypotheses were proposed to explain the observed detonation phenomena of the novel explosive mixtures. It was suggested that the velocity of detonation of these non-ideal explosives is not related to the total amount of energy released during detonation, but is in fact a function of the rate at which explosive energy is released, which in turn is controlled by the activation energies of the explosive reactants. Another hypothesis was that the modelled available energies of the novel explosives were not representative of their true energy released during detonation, due to the hybrid explosives detonating in a non-ideal manner.

Future work is required to fully characterise the detonation performance of the novel explosive mixtures and to test the hypotheses proposed in this paper to explain the observed detonation phenomena. Field testing is required to determine the relative energies of the novel hybrid explosives using standard methods such as underwater testing or crater testing. This would allow analysis of whether the available energies of the novel hybrid explosives estimated by the ideal detonation code were representative of their true available energies during detonation. In order to more thoroughly understand the non-ideal detonation behaviour of the novel explosives, their detonation performance should be tested for a range of charge diameters. The study of hybrid explosives could also be extended to testing novel explosive mixtures containing HP and different nitrates, and testing the influence on detonation performance of alterating the ratios of HP to nitrates in the oxidiser phase.

8 ACKNOWLEDGEMENTS

The authors would like to thank Lee Hayter and the Extech crew for their assistance during the testing program. We would also like to thank Mining3 and the University of Queensland for their support during this work.

REFERENCES

Akhaven, J. 2004. *The Chemistry of Explosives* 2nd ed., London, UK: Royal Society of Chemistry.

Araos, M. & Onederra, I. 2013. Detonation characteristics of alternative mining explosives based on hydrogen peroxide. In *7th World Conference on Explosives & Blasting*. Moscow, Russia: The European Federation of Explosives Engineers.

Araos, M. & Onederra, I. 2015. Development of a novel mining explosive formulation to eliminate nitrogen oxide fumes. *Mining Technology*, 124(1), pp.16–23.

Baker, A. & Groves, W. 1962. Hydrogen Peroxide Explosives, US Patent 3,647,441.

Bouillet, E. *et al*. 1990. Process for the manufacture of explosive cartridges, and explosive cartridges obtained using the said process, US Patent 4,942,800.

Bowden F. & Yoffe A. 1952. Initiation and growth of explosion in liquids and solids. Cambridge University Press, Cambridge, UK.

Braithwaite, M. 2013. Ideal detonation reaction concepts for blasting engineers. In B. Mohanty & V. K. Singh, eds. *Performance of Explosives and New Developments*. London, UK: Taylor & Francis Group, pp. 3–9.

Frost, D. & Zhang, F. 2009. Slurry detonation, *in Shock Wave Science and Technology Reference Library*, Vol. 4, F. Zhang, ed., Springer, New York. pp. 169–216.

Hagan, T. 1968. Performance characteristics of ammonium nitrate/fuel explosives. *PhD Thesis*, School of Engineering, The University of Queensland.

Hattori,K., Fukatsu,Y. & Sakai,H. 1982. The effect of glass microballoon size on the detonation velocity of emulsion explosives. *Journal of Industrial Explosives Society*, 43, pp. 295-301.

Heemskerk, A. & Scholtes, J. 1995. Explodability and detonability of mixtures of hydrogen peroxide and organic matter. In J. Mewis, H. Pasman, & E. De Rademaeker, eds. *8th International Symposium on Loss Prevention and Safety Promotion in the Process Industries*. Antwerp, Belgium, pp. 411–424.

International Society of Explosives Engineers (ISEE), 2014. *ISEE Blasters' Handbook* 18th ed. J. Stiehr, ed., Cleveland, Ohio, USA: Interntional Society of Explosives Engineers.

Lee, J. & Persson, P. 1990. Detonation behaviour of emulsions explosives. *Propellants, Explosives, Pyrotechnics*, 15(5), pp. 208-216.

Lee, J. *et al.* 1989. Detonation and shock initiation properties of emulsion explosives. In *9th International Symposium on Detonation*, Office of Naval Research, Portland, OR, August 28–September 1, 263–271.

Liu, J. 2015. *Liquid Explosives*, Berlin, Germany: Springer.

Mackenzie, J. 1990. Hydrogen peroxide without accidents. *Chemical Engineering*, 97(6), pp. 84–90.

Mahadevan, E. 2013. *Ammonium Nitrate Explosives for Civil Applications*, Chennai, India: John Wiley and Sons Ltd.

MREL, 2017. Microtrap. Available from: http://mrel.com/blasting_instrumentation/microtrap.html

Mohanty, B. 2013. Energetics and performance of modern commercial explosives. In B. Mohanty & V. K. Singh, eds. *Performance of Explosives and New Developments*. London, UK: Taylor & Francis Group, pp. 27–33.

Persson, P., Holmberg, R. & Lee, J. 1993. *Rock blasting and explosives engineering*, CRC Press, Florida, USA.

Price, D. 1966. Contrasting patterns in the behaviour of high explosives. In *11th International Symposium on Combustion*. Berkeley, California, USA: The Combustion Institute, pp. 693–701.

Schreck, A. *et al.* 2004. Investigation of the explosive hazard of mixtures containing hydrogen peroxide and different alcohols. *Journal of Hazardous Materials*, 108(1–2), pp.1–7.

Shanley, E. & Greenspan, F. 1947. Highly concentrated hydrogen peroxide: physical and chemical properties. *Journal of Industrial and Engineering Chemistry*, 39(12), pp.1536–1543.

Shanley, E. & Kauffmann, H. 1948. Peroxide-glycerol explosive, US Patent 2,452,074.

Sheffield, S. *et al.* 2010. Shock initiation and detonation study on high concentration H_2O_2/H_2O solutions using in-situ magnetic gauging. In *14th International Detonation Symposium*. Coeur d'Alene Resort, Idaho, United States, pp. 601–610.

ShotTrack, 2015. ShotTrack VOD Monitor. Available online from: www.shottrack.com.au/ ShotTrack_ VoD.html

Zinn, J. 1962. Initiation of explosions by hot spots. *The Journal of Chemical Physics*, 36(7), pp.1949.